Since January 2020 Elsevier has created a COVID-19 resource centre with free information in English and Mandarin on the novel coronavirus COVID-19. The COVID-19 resource centre is hosted on Elsevier Connect, the company's public news and information website.

Acta Biomaterialia 85 (2019) 203–217

Contents lists available at ScienceDirect

Acta Biomaterialia

journal homepage: www.elsevier.com/locate/actabiomat

Full length article

Size-dependent anti-inflammatory activity of a peptide-gold nanoparticle hybrid *in vitro* and in a mouse model of acute lung injury

Wei Gao [a,1], Yulu Wang [b,1], Ye Xiong [b], Liya Sun [a], Lu Wang [a], Kun Wang [a], Henry Y. Lu [c], Aihua Bao [a], Stuart E. Turvey [c], Qiang Li [a,b,d,*], Hong Yang [a,*]

[a] Department of Pulmonary and Critical Care Medicine, Shanghai General Hospital, Shanghai Jiao Tong University Shool of Medicine, Shanghai 201620, China
[b] Department of Pulmonary and Critical Care Medicine, Changhai Hospital, Second Military Medical University, Shanghai 200433, China
[c] BC Children's Hospital Research Institute, Department of Pediatrics, Faculty of Medicine, University of British Columbia, Vancouver, British Columbia V5Z 4H4, Canada
[d] Department of Pulmonary and Critical Care Medicine, Shanghai East Hospital, Tongji University, Shanghai 200120, China

ARTICLE INFO

Article history:
Received 8 July 2018
Received in revised form 21 December 2018
Accepted 27 December 2018
Available online 28 December 2018

Keywords:
Bioactive nanoparticles
Peptide
Nanodrug
Anti-inflammatory therapeutics
Toll-like receptor signaling
Acute lung injury

ABSTRACT

Acute lung injury (ALI)/acute respiratory distress syndrome (ARDS) is a life-threatening condition of critically-ill patients, characterized by overwhelming inflammatory responses in the lung. Multiple lines of evidence suggest that the excessive activation of Toll-like receptor 4 (TLR4) plays an important role in this detrimental lung inflammation. Recently, we developed a unique class of peptide-gold nanoparticle (GNP) hybrids that act as potent nano-inhibitors of TLR4 signaling by modulating the process of endosomal acidification. In this study, we aimed to identify the key physiochemical factors that could further strengthen the anti-inflammatory activity of these nano-inhibitors, including the nanoparticle size, the density of peptides coating the nanoparticle surface, as well as the number of the effective amino acid phenylalanine (F) residues in the peptide sequence. Among these factors, we found that the nanoparticle size could significantly affect the TLR4 inhibition. Specifically, the peptide-GNP hybrids with a GNP core of 20 nm (P12(G20)) exhibited the most potent inhibitory activity on TLR4 activation and its downstream cytokine production among those with a GNP core of 13 nm (P12(G13)) and 5 nm (P12(G5)) in THP-1 cell-derived macrophages. This size-dependent anti-inflammatory effect of the hybrid P12 was also observed in a lipopolysaccharide (LPS)-induced mouse model of ALI. It was found that P12(G20) was superior to P12(G13) in prolonging the survival of mice experiencing lethal LPS challenge, decreasing the acute lung inflammation, and alleviating diffuse alveolar damage in the lungs. Interestingly, P12(G20) could also promote long-term tolerance to endotoxin. Detailed mechanistic studies demonstrated that when compared to the smaller P12(G13), the larger P12(G20) had higher cellular uptake and a stronger endosomal pH buffering capacity, contributing to its enhanced therapeutic effects on reducing TLR4 activation *in vitro* and *in vivo*. Overall, this study suggests that nanoparticle size is one key factor determining the anti-inflammatory potency of the peptide-GNP hybrids, and the hybrid P12 may serve as a promising, novel class of nanotherapeutics for modulating TLR signaling to treat ALI/ARDS.

Statement of Significance

We have developed a new class of nanoparticle-based inhibitors (i.e., peptide-GNP hybrids) targeting TLR4 signaling in macrophages. Through evidence-based engineering of the nanoparticle size, surface peptide ligand density and effective amino acid (phenylalanine, F) chain length, we identified a peptide-GNP hybrid, P12(G20), with enhanced anti-inflammatory activity. Specifically, P12(G20) was more potent in reducing inflammation in THP-1 cell-derived macrophages and in a LPS-induced ALI mouse model. More interestingly, P12(G20) facilitated long-term protection against lethal LPS challenge *in vivo* and induced endotoxin tolerance *in vitro*. We anticipate that these new hybrids would serve as the next generation anti-inflammatory nano-therapeutics for the treatment of ALI/ARDS or other acute and chronic inflammatory diseases.

* Corresponding authors at: Department of Pulmonary and Critical Care Medicine, Shanghai General Hospital, Shanghai Jiao Tong University Shool of Medicine, Shanghai 201620, China (Q. Li and H. Yang).
E-mail addresses: liqressh@hotmail.com (Q. Li), hongyang36@gmail.com (H. Yang).
[1] W.G. and Y.W. contributed equally to the paper.

https://doi.org/10.1016/j.actbio.2018.12.046
1742-7061/

1. Introduction

Acute lung injury (ALI), a mild form of acute respiratory distress syndrome (ARDS), is a complex syndrome that can rapidly develop into life-threatening acute hypoxemic respiratory failure [1]. ALI/ARDS is defined as an overwhelming inflammatory process in lungs characterized by cytokine storm, neutrophil infiltration, diffuse endothelium damage, increased vascular permeability and gas exchange impairment, eventually leading to respiratory failure with a high mortality rate [2,3]. Although significant efforts have been made in understanding the disease pathophysiology and developing treatments for ALI/ARDS, very few pharmacotherapies have shown clinical efficacy in reducing the mortality rate [4]. In fact, of all potential interventions, only low tidal volume mechanical ventilation has been proved to be clinically beneficial for the patients. Therefore, developing novel therapeutic approaches to manage the excessive inflammatory responses in ALI/ARDS is an unmet clinical need.

One pharmacologic strategy to manage the excessive inflammation in ALI/ARDS is to regulate over activation of Toll-like receptors (TLRs), which represents an important pathogenic factor of ALI/ARDS [5]. Among all TLRs discovered in humans, TLR4 appears to play a central role in both infectious and non-infectious lung inflammation and injury [6,7]. In the past decades, various TLR4 antagonists were developed [8], including small molecule inhibitors (e.g., TAK-242) [9], lipid-A analogs (e.g., Eritoran, E5564) [10], antibodies (e.g., NI-0101) [11] and microRNAs (e.g., miR-146a) [12]. Although they showed excellent inhibitory efficacy in pre-clinical studies and some were advanced into clinical trials, to date none have been approved for clinical use. The pathogenic complexity (e.g., multiple TLR pathways are often involved) of both infection and non-infection associated ALI/ARDS is probably one major reason for these failures in drug development.

The rapid advances in nano-science and technology have created diverse materials with various surface chemistry and properties, providing unconventional approaches to treat human diseases [13–17]. These nanoscale materials, particularly nanoparticles, have unique sizes (e.g., 10–200 nm) that allow for enhanced cellular uptake and preferred biodistribution [18,19]; they have a large surface area that can be rationally functionalized to reprogram their surface properties to improve the biodistribution (PEGylation) [20], achieve tissue/cell targeting (antibodies) [21], and sustain the cargo release [22]. Thus, nanoparticles have been widely applied as drug carriers to enhance the therapeutic potential of the conventional drugs. On the other hand, bioactive nanoparticles have recently been applied to manipulate immune responses as new immunotherapies [8,14,23]. By changing their surface properties, nanoparticles can either boost antigen specific immune responses for vaccine development [24], or alternatively, be used to suppress immune responses during transplantation or in autoimmune diseases [15,25,26]. Regulation of TLR signaling using thoughtfully designed nanodevices may represent a novel therapeutic approach to combat the overwhelming inflammatory responses in ALI/ARDS.

Owing to their unique properties for better therapeutic outcomes, nanodevices are emerging as a new class of potent TLR inhibitors. For example, by conjugating bioactive molecules, such as non-anticoagulant heparin (NAH) [27,28] and high-density lipoprotein (HDL), onto nanoparticles, these novel nanodevices were able to sequester the inflammatory mediators (cytokines) or the TLR agonist like lipopolysaccharide (LPS) [29] to reduce the inflammatory responses triggered by TLR4 activation. Instead of loading bioactive compounds onto the nanoparticles, we have developed a unique class of peptide-gold nanoparticle (GNP) hybrids that are made of a GNP core coated with hexapeptides [30,31]. Both components are individually incapable of TLR inhibition, but after their formation into peptide-GNP hybrids they exhibit potent activity in reducing TLR signaling. In addition, the peptide coatings stabilize the GNPs at physiological conditions and allow the convenient adjustment of the surface chemistry of the hybrids to control their cellular uptake and anti-inflammatory activity [31,32]. Importantly, these hybrids are capable of inhibiting multiple TLR signaling pathways in macrophages [31,33], which are the key players in the inflammatory responses of ALI/ARDS.

In this study, we aimed to further optimize the anti-inflammatory activity of the hybrids for future clinical translation by fine tuning three important factors: the nanoparticle size, the density of the peptide coatings and the number of the effective amino acid (phenylalanine, F) in the coated peptide sequence. Their effects on TLR4 inhibition were examined using various *in vitro* methods. We then investigated the *in vivo* efficacy of the best optimized hybrids and assessed their clinical translational potential using a classical LPS-induced ALI murine model. This work provides essential knowledge about factors that determine the efficacy of peptide-GNP hybrids in inhibiting inflammation *in vitro* and *in vivo*, and aids to the development of an effective novel nano-therapy to ameliorate the devastating inflammation in ALI/ARDS.

2. Results

It is well-known that unmodified or bare GNPs (usually coated with citrate after synthesis) are not stable and tend to aggregate at physiological condition, i.e., 0.9% saline, which largely limits their biomedical applications. Previously, we developed a strategy to modify the GNP surface using hexapeptides, not only to stabilize GNPs at physiological conditions but also enable programing of the surface chemistry of GNPs by altering the amino acids in the peptide sequence. These modifications created a new class of peptide-GNP hybrids with exciting bioactivities to modulate immune responses [30,31,34]. Among the newly created peptide-GNP hybrids, we identified a unique lead hybrid–designated P12–capable of potently inhibiting TLR4 signaling and primarily targeting phagocytic cells (e.g., macrophages) [31,32]. P12 is made of 13-nm GNPs coated with a hexapeptide (peptide sequence: CLPFFD) as schematically illustrated in Fig. 1a. Surprisingly, the substitution of the two phenylalanine residuals (FF) in the hexapeptides on P12 with alanine (AA) rendered the hybrid (designated P13) inactive. Since P13 has almost identical physicochemical properties as P12, it can serve as an optimal inactive control hybrid for experimental comparisons.

Our earlier work suggested that the immune modulatory activity of P12 was highly dependent on its cellular uptake and the buffering effect to neutralize protons in the endosomal compartment during acidification [32]. In addition, the two F residues also played an important role in "tuning" the bioactivity of the hybrids [31,32]. To further optimize the inhibitory and anti-inflammatory activity of P12, we thus manipulated three key physicochemical factors that may facilitate the uptake and pH neutralization, including the nanoparticle size, the peptide density on the hybrid surface, and the number of F residues in the peptide sequence. The impacts of these key factors on the inhibitory and anti-inflammatory activity were first examined *in vitro*; the promising strategy was then validated *in vivo* using an ALI mouse model.

2.1. Nanoparticle size determines the inhibitory and anti-inflammatory activity of the hybrid in vitro

We first examined the effect of the nanoparticle size on the inhibition of TLR4 signaling and the associated inflammatory

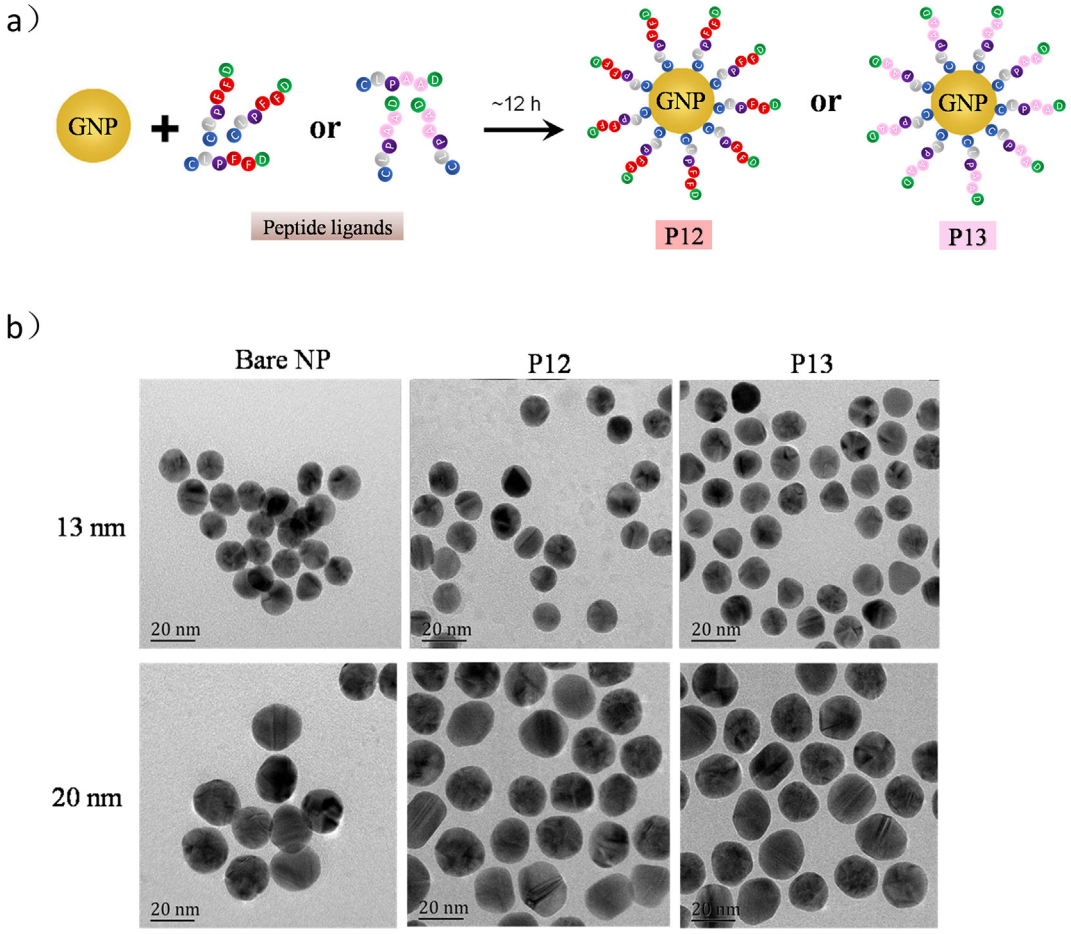

Fig. 1. Fabrication and characterization of bare GNPs and peptide-GNP hybrids with different sizes. (a) A schematic diagram of the peptide-GNP hybrid (P12 and P13) fabrication. (b) TEM images of bare GNPs and various peptide-GNP hybrids with different sizes of the GNP core. Scale bar: 20 nm.

response. Two different sizes of the P12 hybrids, P12(G13) and P12 (G20), were first studied; they were made of 13-nm (G13) and 20-nm (G20) diameter GNP cores. The two control inactive hybrids were also fabricated corresponding to the GNP core sizes as P13 (G13) and P13(G20). The size and morphology of the bare GNPs and the hybrids were characterized by the transmission electron microscopy (TEM) (Fig. 1b). The sizes of the synthesized GNP cores were confirmed to be 13.0 nm and 19.7 nm (in diameter) for G13 and G20, respectively (Table 1). The surface modification by the peptide coatings did not change the morphology and size of the GNPs under TEM (Fig. 1b). However, as expected the hydrodynamic diameter of the hybrids is slightly bigger (increased 1–2 nm) than that of the bare GNPs, consistent with the presence of the peptides coating the nanoparticles (Table 1).

To investigate how the nanoparticle size affects the inhibitory activity of the hybrids on the TLR4 signaling, we employed a reporter cell system to monitor the activation of the both arms of TLR4 pathway cascade (NF-κB/AP-1 and IRF activation) as described in our earlier work [31]. As shown in Fig. 2a, b and Fig. S1, at the same molar concentration, P12(G20) exhibited more potent inhibitory activity than P12(G13) on both NF-κB and IRF activation upon LPS (10 ng/mL) stimulation. On the contrary, the control nanoparticles P13(G13) and P13(G20) had no inhibitory activity at all regardless their differences in the size. The inhibitory effect of P12(G20) and P12(G13) on the NF-κB and IRF activation was also observed by immunoblotting (Fig. 2c and d). Both P12(G20) and P12(G13) could significantly reduce p65 phosphorylation and IκBα degradation, indicating their inhibitory activity on NF-κB activation. Their inhibition on IRF3 were seen by the decrease in the IRF3 phosphorylation. Comparing to P12(G13), P12(G20) showed slightly higher inhibitory activity on the p65 and IRF3 phosphorylation.

Table 1
Quantitative analysis of the size of bare GNP and the hybrids by TEM and DLS.

Nanoparticles	Size by TEM (nm) ± SD	Hydrodynamic diameter (nm) ± SD	PDI (nm) ± SD
Bare 13-nm GNP	13.0 ± 0.6	18.7 ± 0.7	0.26 ± 0.01
P12(G13)	13.0 ± 0.8	19.7 ± 0.2	0.25 ± 0.01
P13(G13)	13.1 ± 0.8	20.8 ± 1.1	0.27 ± 0.01
Bare 20-nm GNP	19.7 ± 1.4	24.8 ± 0.5	0.21 ± 0.01
P12(G20)	19.7 ± 1.2	26.9 ± 0.8	0.17 ± 0.02
P13(G20)	19.8 ± 1.3	26.6 ± 2.0	0.17 ± 0.05

PDI: polydispersity index.

The anti-inflammatory activity of the hybrids was accessed by measuring the release of two key cytokines CCL2 and CCL4 in the THP-1 derived macrophages after LPS stimulation (Fig. 2e and f). Consistent with the TLR4 inhibition profile seen in the reporter cells, P12(G20) exhibited much stronger inhibition on CCL2 and CCL4 secretion than P12(G13), while the inactive hybrid controls P13(G13) and P13(G20) did not have significant inhibitory effect. These hybrids did not exhibit cellular toxicity at the experimental concentrations (Fig. S2).

In order to generalize the size effect, we then employed other four sizes of the P12 hybrids, P12(G5), P12(G30), P12(G40) and P12(G50), made of 5-nm, 30-nm, 40-nm and 50-nm diameter GNP cores, respectively. The morphology and size of the hybrids

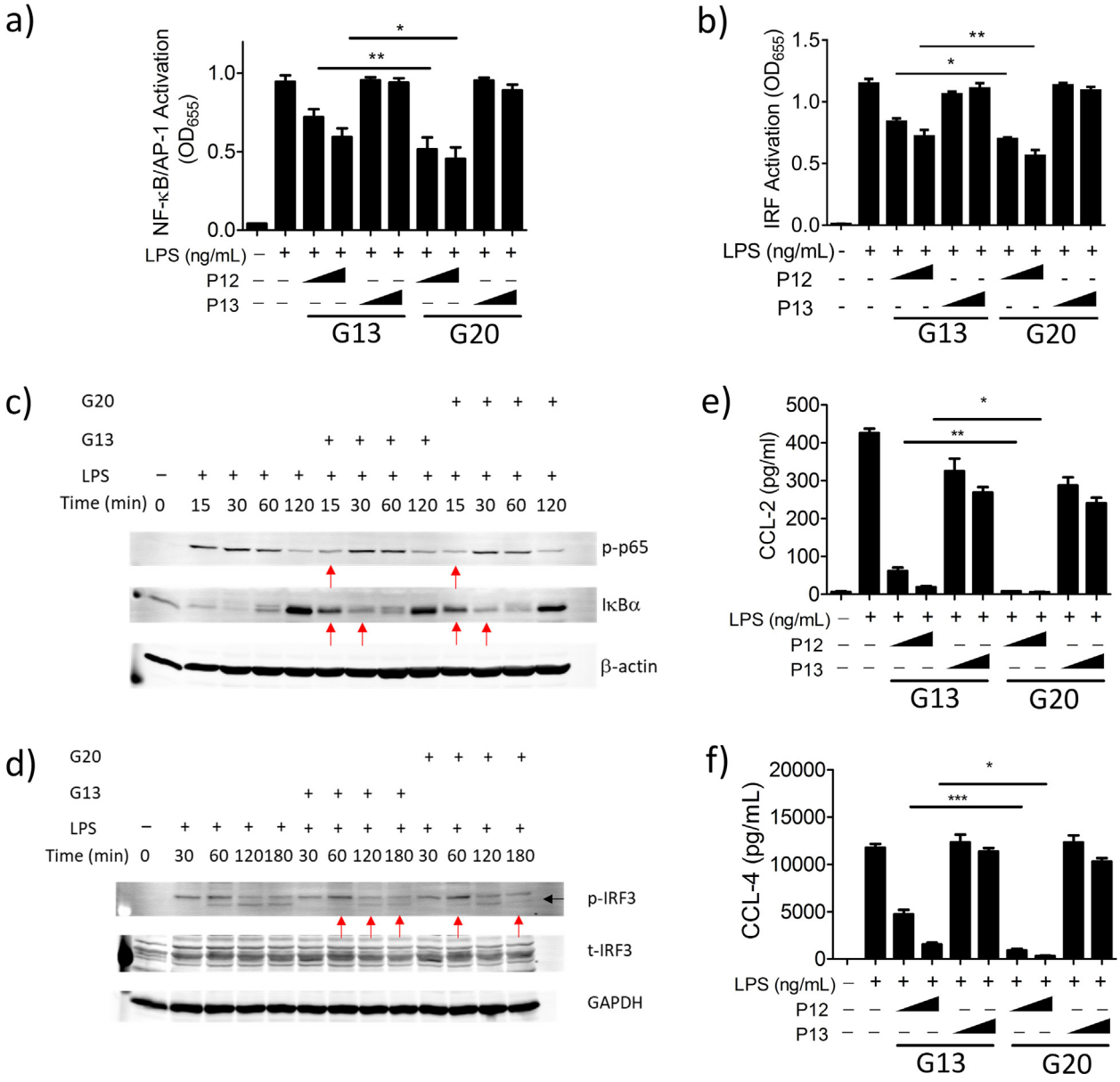

Fig. 2. Nanoparticle size determines their inhibitory activity on TLR4 signaling in THP-1 cell-derived macrophages. (a and b) Inhibition of NF-κB/AP-1 (a) and IRF (b) activation by P12(G20) upon LPS stimulation in comparison with P12(G13) and the inactive P13. Hybrid concentrations: 50 nM and 100 nM. (c and d) Immunoblots validating the inhibitory effect of P12(G20) and P12(G13) on (c) the phosphorylation of p65 (p-p65) and IκBα degradation for NF-κB activation and (d) phosphorylation of IRF3 (p-IRF3) for IRF activation; black arrows indicated the p-IRF3 band and red ones indicated the differences comparing to LPS only. Hybrid concentrations: 50 nM. (e and f) Inhibition of the LPS-induced cytokines CCL2 (e) and CCL4 (f) production in THP-1 cell-derived macrophages by the hybrids P12(G20) and P12(G13). Hybrid concentrations: 50 nM and 100 nM. LPS = 10 ng/mL, N ≥ 3, *p < 0.05, **p < 0.01, ***p < 0.001. (For interpretation of the references to color in this figure legend, the reader is referred to the web version of this article.)

were characterized by the TEM (Fig. S3a), where the sizes of the GNP cores were quantified to be 5.2 ± 0.4 nm, 30.5 ± 1.5 nm, 40.6 ± 1.5 nm and 49.6 ± 3.4 nm (in diameter) for P12(G5), P12 (G30), P12(G40) and P12(G50), respectively. While P12(G5) was physiologically stable in 0.9% saline (150 mM NaCl solution), P12 (G30), P12(G40) and P12(G50) were not (Fig. S3b–j); as a result, these three hybrids were not proceeded for further studies. The *in vitro* evaluation revealed that the inhibitory activity of P12(G5) on LPS-induced NF-κB/AP-1 and IRF activation, as well as CCL2 secretion was significantly lower than P12(G13) at the same molar concentration (50 nM) or equivalent surface area (338 nM) (Fig. S4). Collectively, these data suggested that the inhibitory and anti-inflammatory activity of P12 was nanoparticle size dependent: P12(G20) > P12(G13) ≫ P12(G5).

2.2. The effect of coated peptide density and the phenylalanine number in the peptide sequence on the anti-inflammatory activity of the peptide-GNP hybrids

We previously showed that the surface modification of the GNPs with specific hexapeptides enhanced the cellular uptake and enabled the endosomal pH modulatory activity, contributing to the novel TLR inhibitory activity of the hybrid P12 [32]. Such effects could be attributed to the hydrophobic phenylalanine (FF) residues and the end negatively charged aspartic acid (D) residues in the peptide sequence [31,32]. Thus, it is reasonable to hypothesize that increasing the density of the peptides coated on the GNP surface may further facilitate the anti-inflammatory activity of P12. This was achieved by the addition of NaCl salt during the

conjugation process to screen the charges and reduce the repulsive interaction between peptides, allowing more peptides conjugating to the GNP to form a denser peptide coating on the surface, as illustrated in Fig. 3a. Comparing to no salt formulation process, the addition of 300–500 mM NaCl during peptide conjugation indeed increased the physiological stability of the hybrids in high salt (NaCl) solution (Fig. 3b), indicating that these hybrids had a denser peptide coating on the GNP surface. However, the new hybrid P12 (NaCl 500 mM) with a denser peptide coating did not exhibit a stronger inhibitory activity on LPS-induced NF-κB/AP-1 activation and the downstream CCL2 cytokine secretion in comparison with the original P12 formulated without salt addition (Fig. 3c and d).

Since F residues of the peptide ligands were found to be crucial to the anti-inflammatory activity of P12 from our previous study

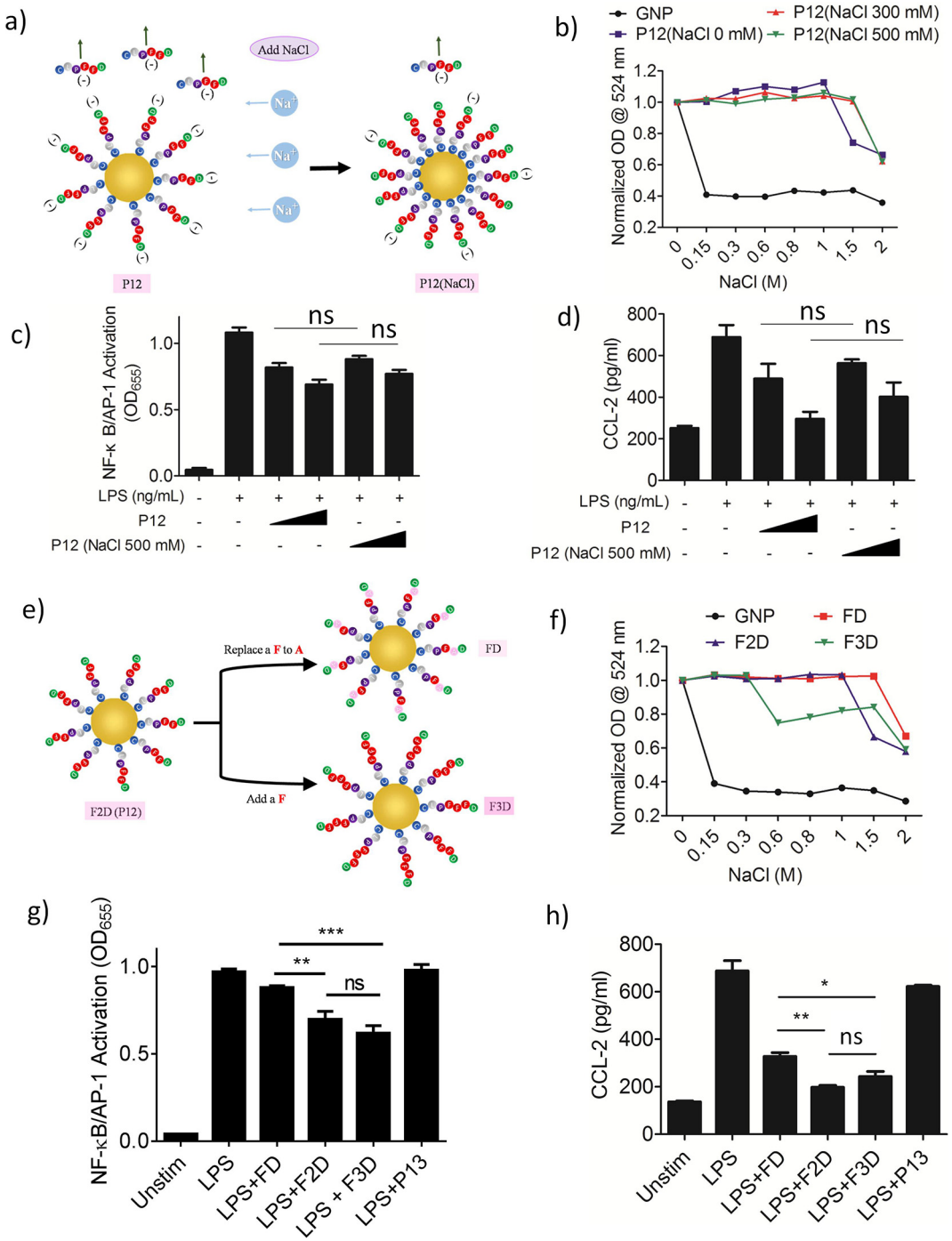

Fig. 3. Effect of the peptide density on the GNP surface and the number of phenylalanine residues (F) in the peptide sequence on TLR4 signaling in THP-1 cell-derived macrophages. (a) A scheme showing the procedure of increasing the peptide density on the GNP surface by adding NaCl during peptide conjugation to the GNPs. (b) Stability of P12 with or without the addition of NaCl (300 mM and 500 mM) during conjugation in NaCl solutions with various concentrations (0–2 M). (c and d) Inhibition of NF-κB activation (c) and CCL2 production (d) upon LPS stimulation by P12 fabricated with or without NaCl addition (500 mM). (e) A scheme illustrating the hybrids formed with different numbers of F in the peptide sequence. FD: CLPFAD; F2D: CLPFFD or P12; F3D: CLPFFFD. (f) Stability of FD, F2D (P12) and F3D in NaCl solutions with different concentrations (0–2 M). (g and h) Inhibition of NF-κB activation (g) and CCL2 production (h) upon LPS stimulation by the new hybrids of FD and F3D in comparison with F2D (P12). Nanoparticle concentration = 100 nM, LPS = 10 ng/mL, N ≥ 3, *p < 0.05, **p < 0.01, ***p < 0.001.

[31], it may be possible to tune such an activity by altering the number of F in the peptide sequence. To test this hypothesis, three peptide sequences were designed: CLPFAD (FD, with a single F in the peptide), CLPFFD (F2D = P12, with two F) and CLPFFFD (F3D, with three F) (Fig. 3e). We first characterized the stability of these new hybrids in NaCl solutions. We found that the hybrid FD was more stable than P12 (F2D), while F3D was the least stable (Fig. 3f). This trend was reasonable as more hydrophobic F residues on the GNP surface would increase the hybrid hydrophobicity, promoting the nanoparticle interaction to form aggregates. We next evaluated the *in vitro* inhibitory activity of these three hybrids using NF-κB/AP-1 reporter cells. We found that both F2D and F3D significantly reduced the NF-κB/AP-1 activation, while FD did not (Fig. 3g). No big difference in the inhibitory activity was observed between F2D and F3D. Interestingly, all three hybrids were able to decrease LPS-induced CCL2 production, where F3D and F2D displayed similar inhibitory activity stronger than FD (Fig. 3h). Although these results suggested that F residues are important for the inhibitory activity of the hybrids (F3D and F2D vs. FD), the addition of more F (F3D vs. F2D) did not help further enhance such inhibitory effects. We further validated this finding in a LPS-induced ALI mouse model; the results confirmed that F3D treatment had a comparable effect as F2D treatment on reducing the lung inflammation (Fig. S5a–d). Taken together, our data indicated that neither changing peptide density on the GNP surface nor increasing the number of F in the peptide sequence could enhance the inhibitory activity of the hybrid P12 *in vitro* and *in vivo*.

2.3. Enhanced therapeutic activity of P12(G20) in a LPS-induced ALI mouse model

Since P12(G20) showed a stronger ability in inhibiting TLR4 signaling and cytokine production *in vitro* than P12(G13), we anticipated that P12(G20) may be more effective on reducing LPS triggered inflammation *in vivo*. To test this hypothesis, we adopted a LPS-induced ALI mouse model to mimic the acute inflammatory phase of ALI/ARDS. The mice were challenged with a nonlethal dose of LPS (10 mg/kg) intranasally to cause acute lung inflammation; the treatments P12(G20), P12(G13) and the inactive control nanoparticle P13(G13) were given 1 h before the LPS challenge via intratracheal instillation, and the analyses were performed 24 h after LPS stimulation (Fig. 4a).

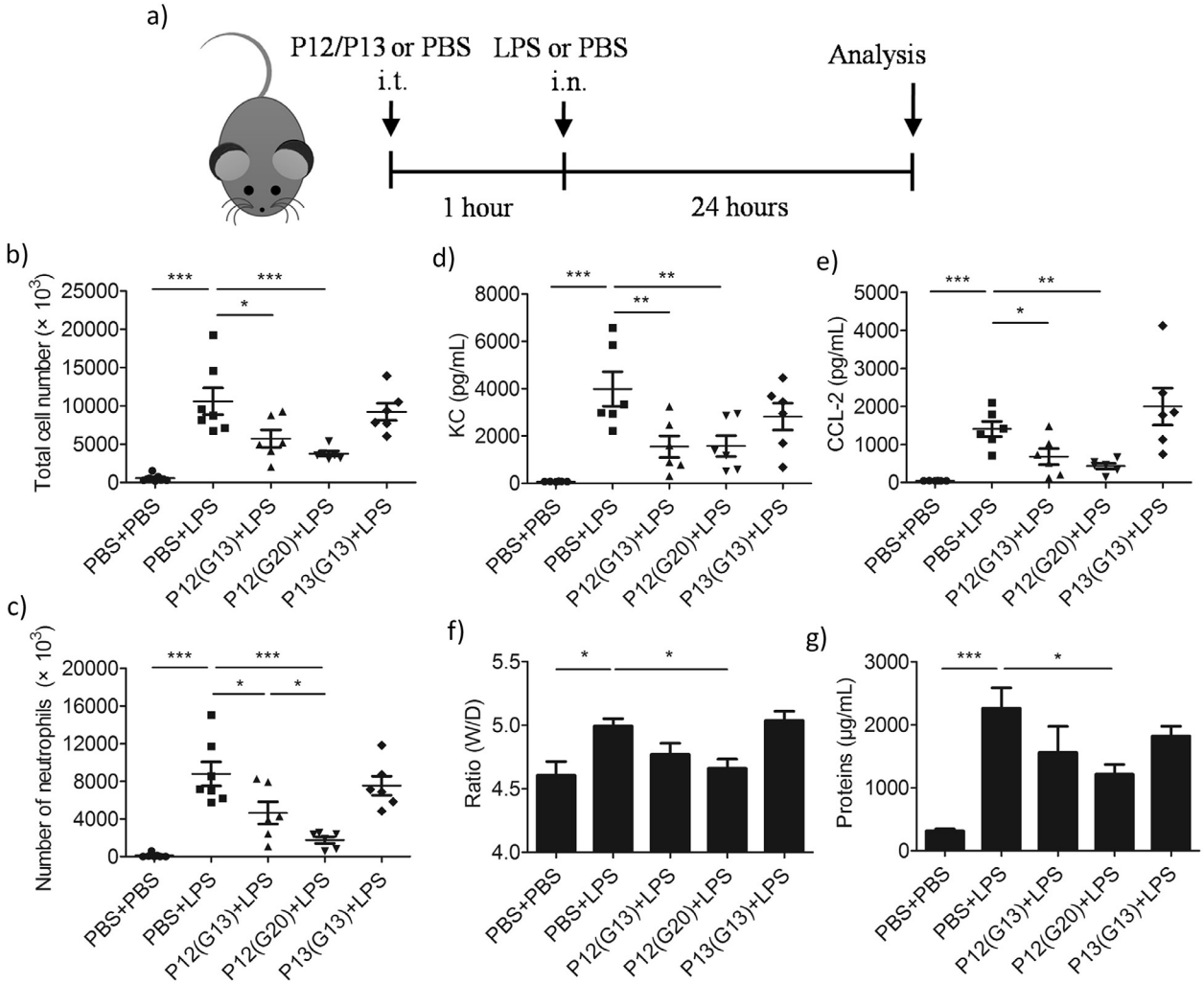

Fig. 4. The inhibitory activity of P12(G20) and P12(G13) in a LPS-induced ALI mouse model. (a) The LPS-induced ALI mouse model with the pretreatment of the hybrids P12 (G20), P12(G13) and P13. The hybrids (50 μL) were given via intratracheal injection (i.t.) 1 h before the LPS challenge via nasal inhalation; mice were sacrifice for analysis 24 h after LPS stimulation. The BALF was collected for the analysis of the total cell counts (b), neutrophil counts (c) and cytokines KC (d) and CCL2 (e) production. The permeability of the alveolocapillary membrane was evaluated by the lung wet/dry (W/D) ratio (f) and the total protein amounts in the BALF (g). Nanoparticle concentration = 25 pmol per mouse, LPS = 10 mg/kg per mice, N ≥ 6 per group, *p < 0.05, **p < 0.01, ***p < 0.001.

The lung inflammation was first assessed by analyzing the cell infiltration and cytokine secretion in the bronchoalveolar lavage fluid (BALF). It was found that both P12(G20) and P12(G13) significantly decreased the numbers of total inflammatory cells and neutrophils in the BALF, but P13(G13) did not (Fig. 4b and c); comparing to P12(G13), P12(G20) exerted a stronger inhibitory action in neutrophil recruitment (Fig. 4c). Both sizes of P12 also significantly reduced the levels of the neutrophil chemotactic cytokine KC and the monocyte/macrophage chemotactic cytokine CCL2 in the BALF (Fig. 4d and e). The permeability of the alveolocapillary membrane in the pathogenesis of ALI was then accessed by measuring the BAL total proteins and the ratio of wet lung to dry lung (W/D ratio). It was found that only P12(G20) treatment was able to significantly decrease W/D ratio and total proteins in the BALF (Fig. 4f and g). These results demonstrated that P12(G20) was more potent than P12(G13) in the management of lung inflammation.

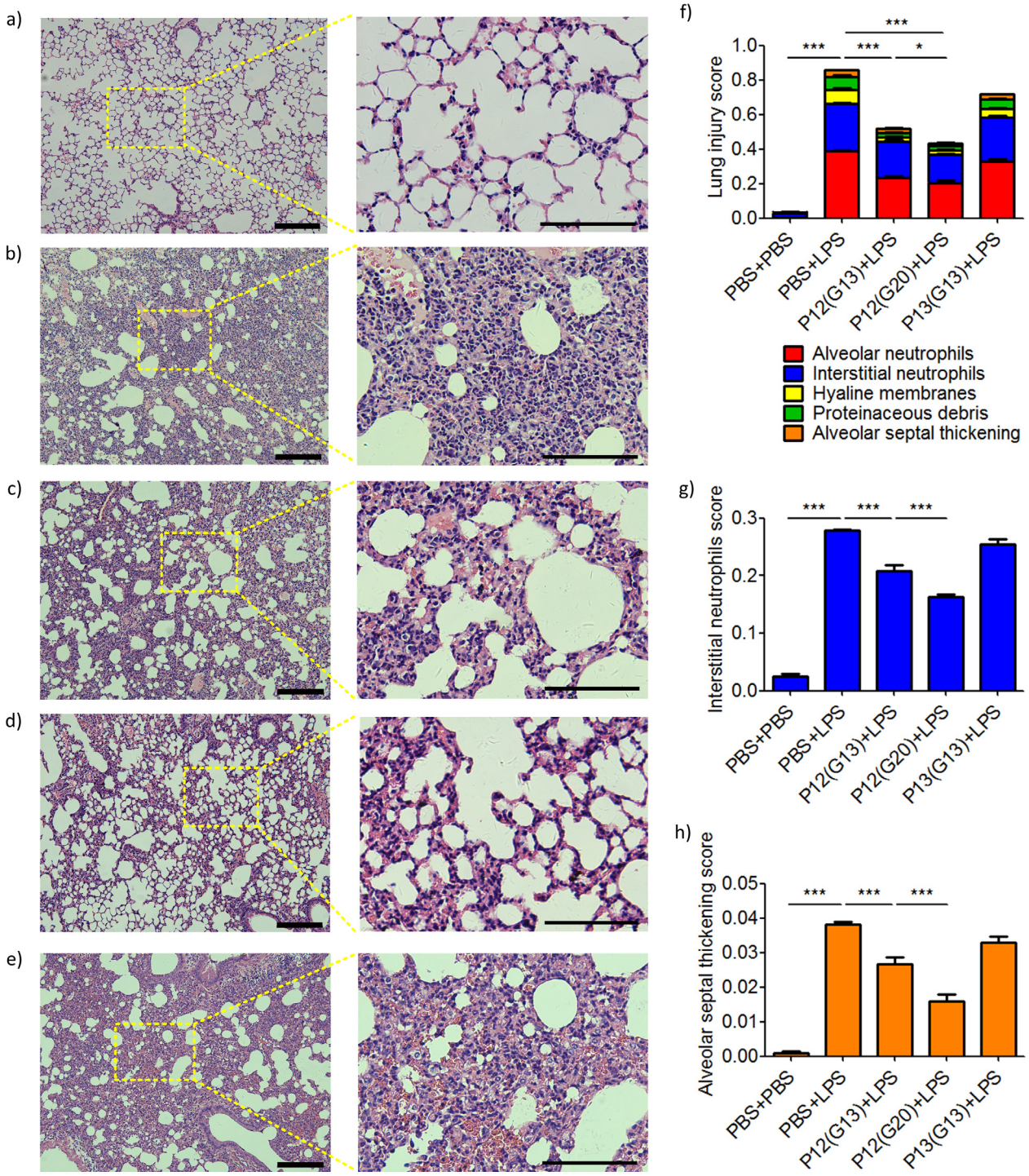

Fig. 5. The protective effect of the peptide-GNP hybrids P12(G20) and P12(G13) on lung damages in LPS-induced ALI mice. (a–e) The representative histological images of H&E stained lung sections 24 h after LPS stimulation: (a) sham control (PBS only), (b) PBS + LPS, (c) P12(G13) + LPS, (d) P12(G20) + LPS, (e) P13(G13) + LPS. The scale bar in the left panel = 200 μm while that in the right panel = 100 μm. The lung damages were accessed by 5 pathophysiological features to obtain the total injury score (f). The hybrids P12(G13) and P12(G20) significantly reduced the number of neutrophils in the interstitial space (g), and alveolar septal thickening (h). N ≥ 6 per group, *p < 0.05, ***p < 0.001.

In parallel to BAL analysis, we also examined the effects of the hybrids on the lung injury levels assessed from the lung tissue histopathology. The lung injury was manifested by neutrophils in the alveolar space, neutrophils in the interstitial space, hyaline membrane formation, proteinaceous debris filling the airspaces and alveolar septal thickening (Fig. 5a–e), and the lung injury score was obtained based on these features. It was found that the average injury score of P12(G20) treated group was significantly lower than that of the P12(G13) treated group (Fig. 5f). Specifically, P12 (G20) treatment resulted in less interstitial neutrophils and alveolar septal thickening than P12(G13) (Fig. 5g and h). These data suggested that P12(G20) was superior to P12(G13) in inhibiting inflammatory responses and reducing diffuse alveolar damage in lungs with ALI.

Next, we examined the protective effect of P12(G20) on the short-term and long-term survival rate using lethal doses of LPS (20 and 25 mg/kg) (Fig. 6a). The treatments were given 1 h prior to the LPS challenge (20 mg/kg), and the body weight and survival status of the mice were recorded every day. As shown in Fig. 6b, P12(G20) treated mice had a significantly higher survival rate (close to 90%) than P12(G13) treated ones (~75%). In addition, the weight loss of P12(G20) pretreated group was likely reduced (Fig. S6). Since P12(G20) has a surface area 2.4 times larger than P12(G13), the observed enhanced protective effects by P12(G20) may be due to its larger surface. To control for this factor, we increased the dose of P12(G13) to 3 nmol/kg to achieve equivalent surface area of P12(G20) (1.25 nmol/kg). Even at the same surface area, P12(G20) still exhibited a stronger protective effect than P12 (G13) (Fig. 6c), indicating that the nanoparticle size indeed played an important role in modulating the therapeutic activity of P12. Surprisingly, we observed that P12(G20)-treated mice that survived the first endotoxic shock developed a long-term tolerance to a second lethal LPS challenge (25 mg/kg) (Fig. 6d). This phenomenon only occurred with the bigger P12(G20) but not with the smaller P12(G13) regardless at the same molar concentration or surface area to G12(P20). The biodistribution of the two hybrids in mice 1 month post administration was also analyzed (Fig. S7). It was found that both hybrids tend to locate in the lung and mediastinal lymph nodes than other organs; comparing to P12(G13), P12(G20) had even lower accumulation in the mononuclear phagocyte system (MPS), such as liver, spleen and bone marrow. These results indicated that P12(G20) was capable of increasing the short-term survival rate, inducing a long-term protective effect to LPS challenge as well as minimizing the hepatic side-effects, suggesting a promising clinical application of the developed peptide GNP hybrids for treating ALI/ARDS.

2.4. P12(G20) could enhance LPS tolerance in vitro

From the *in vivo* studies, we observed that P12(G20) could enhance the long-term protective effect against the 2nd LPS challenge. Such a striking phenomenon may be rationalized by the capability of P12(G20) promoting the LPS tolerance. LPS tolerance, or endotoxin tolerance (ET) is a state of repressed responsiveness to repeated LPS stimulation, which may serve as a protective mechanism to avoid overwhelming immune responses due to continuous and repeated endotoxin exposure. To test this hypothesis *in vitro*, we used the THP-1 derived macrophages with a reporter system of NF-κB/AP-1 or IRF activation to monitor the LPS tolerance effect. The cells were first stimulated with LPS (10 ng/ml) for 24 h in the presence and absence of P12(G20) or P12(G13); they were then rested for 6, 24 or 48 h prior to the second LPS exposure (10 ng/ml) for another 24-h period. The NF-κB/AP-1 or IRF activation was quantified by measuring the reporter enzymatic reaction using a colorimetric assay (Fig. S8). It was found that LPS pretreated cells exhibited tolerance to the second LPS stimulation, where the activation of NF-κB/AP-1 was significantly reduced compared to one-time LPS exposure (Fig. 7). Without an intervention, the tolerance effect was gradually diminished with the increase in the resting time (Fig. 7b and c), where the inhibition

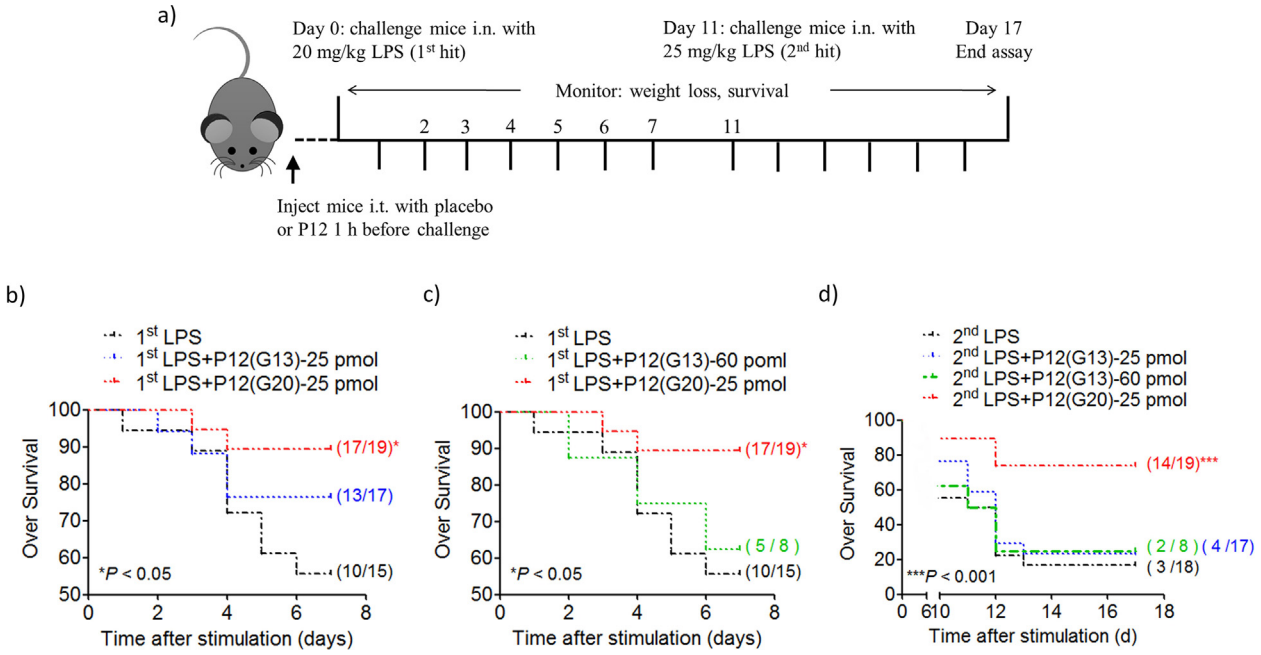

Fig. 6. Effect of the peptide-GNP hybrids P12(G20) and P12(G13) on the short-term and long-term survival in LPS-induced ALI mice. (a) A scheme of the prophylactic treatments of P12(G20) or P12(G13) in a LPS-induced ALI model. The mice were pretreated with the hybrids or PBS intratracheally 1 h before the first LPS challenge (20 mg/kg) at Day 0, and the survived mice were given a second dose (25 mg/kg) of LPS at Day 11. (b and c) The nanoparticle size effects of P12(G20) comparing to P12(G13) on the short-term survival of the severe ALI mice at the same molar concentration of 25 pmol per mouse (b) or the same effective surface area (25 pmol P12(G20) vs. 60 pmol P12 (G13) per mouse (c). (d) The long-term survival of severe ALI mice after secondary LPS challenge with the prophylactic treatments of the hybrids P12(G20) and P12(G13). $N \geq 8$ per group, *$p < 0.05$ vs. PBS + LPS group, ***$p < 0.001$ vs. PBS + LPS + LPS group.

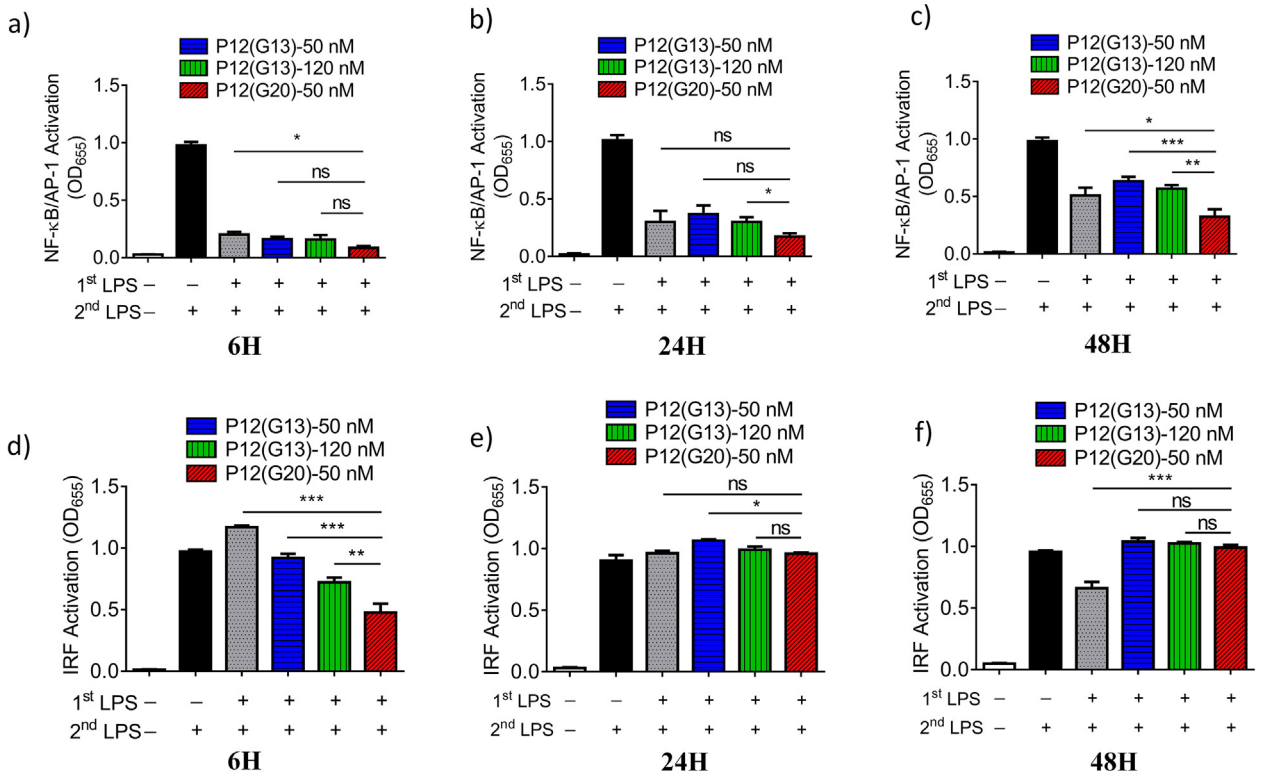

Fig. 7. The enhanced LPS tolerance effect by P12(G20) in the reporter THP-1 cell-derived macrophages. Inhibition of NF-κB activation (a–c) and IRF activation (d–f) by P12 (G20) comparing to P12(G13) upon the second LPS exposure at 6 h (a and d), 24 h (b and e) and 48 h (c and f) after the first LPS stimulation. N = 4, $^{*}p < 0.05$, $^{**}p < 0.01$, $^{***}p < 0.001$.

of NF-κ/AP-1 activation decreased from 80% to 40% as the resting time increase from 6 h to 48 h, respectively. Interestingly, we found that only with the presence of P12(G20) during the first LPS exposure, the cells responded less in NF-κB/AP-1 activation upon the second LPS stimulation comparing to non-hybrid and P12(G13) treatment groups (Fig. 7a–c). For IRF activation, the LPS tolerance effect was more pronounced for P12(G20) comparing to P12(G13) at 6 h rest (Fig. 7d); with longer resting time (24 and 48 h), the tolerance effect disappeared (Fig. 7e and f). Interestingly, only larger P12(G20) show an enhanced LPS tolerance effect in both arm of signaling pathways, while P12(G13) could not no matter it is at the same concentration or same surface area to P12 (G20). This observation suggested that the nanoparticle size is important to induce stronger ET *in vitro*, supporting our *in vivo* findings (Fig. 6).

2.5. The mechanism(s) of action for the nanoparticle size enhanced anti-inflammatory activity of P12

For endosomal TLRs and TLR4, the pH of the endosome is critical for their signal transduction [35–37]. Therefore, modulation of endosomal pH provides a unique way to control TLR signaling. Previously, we discovered that the high cellular uptake of P12 and the blockade of the acidification process in endosomes contributed to the potent inhibition on TLR4 signaling [32]. Since we observed an enhanced inhibitory activity of P12(G20) comparing to P12 (G13), we hypothesized that P12(G20) probably had even higher cellular uptake than P12(G13), contributing to a stronger blockade of the endosomal acidification and more potent inhibition on TLR4 signaling. To test this hypothesis, we first established the relationship between cellular uptake and the anti-inflammatory activity of P12(G13) (Fig. 8a,b and Fig. S9). By using the endocytosis inhibitor cytochalasin D (Cyto D) and the class A scavenger receptor inhibitor fucoidan, we found that the reduction of the nanoparticle uptake can diminish the anti-inflammatory activity, suggesting that cellular uptake is one key factor determining the anti-inflammatory activity of P12(G13). We then employed ICP-MS method to quantify the cellular uptake of P12(G13) and P12(G20) at 12 and 24 h into THP-1 cells-derived macrophages. As shown in Fig. 8c, the uptake of P12(G20) was 266.2×10^5/cell, which was significantly higher than that of P12(G13) (8.5×10^5/cell, $p < 0.001$) at 12 h. Interestingly, the inactive control hybrid P13(G20) also had higher uptake than P13(G13) (Fig. S10), indicating that these macrophages had preferential internalization of 20-nm nanoparticles than the 13-nm ones. A similar trend was observed at 24 h as well. These results indicated that the nanoparticle size is critical for the cellular uptake of the hybrids. This was further confirmed in the ALI mice (24 h after LPS challenging), where the uptake of P12(G20) in the alveolar macrophages (from the BALF) was significantly higher than that of P12(G13) at the same molar concentration or equivalent surface area (Fig. 8d) using the ICP-MS technique.

Next, we investigated whether the high uptake of P12(G20) in THP-1 derived macrophages was indeed more potent in blocking the endosomal acidification than P12(G13). We first compared the buffering capability between P12(G20) and P12(G13) in test tubes by measuring their pH titration curves at the same concentration of 20 nM. Comparing to the saline (0.9% NaCl) solution, both P12(G13) and P12(G20) exhibited a buffering effect between pH 4 and pH 6, and the buffering capacity of P12(G20) was much higher than that of P12(G13) (Fig. 8e). This suggested that P12 (G20) could exert a more potent regulatory activity in the endosomal pH range (pH 4.5–6) when internalized into target cells. To confirm this, we employed a pH-sensitive fluorescence probe, pHrodo red-labeled dextran (10,000 MW), to measure the endosomal pH alteration in the cells [38]; when the endosomal pH increases, the emission intensity of pHrodo-red gradually

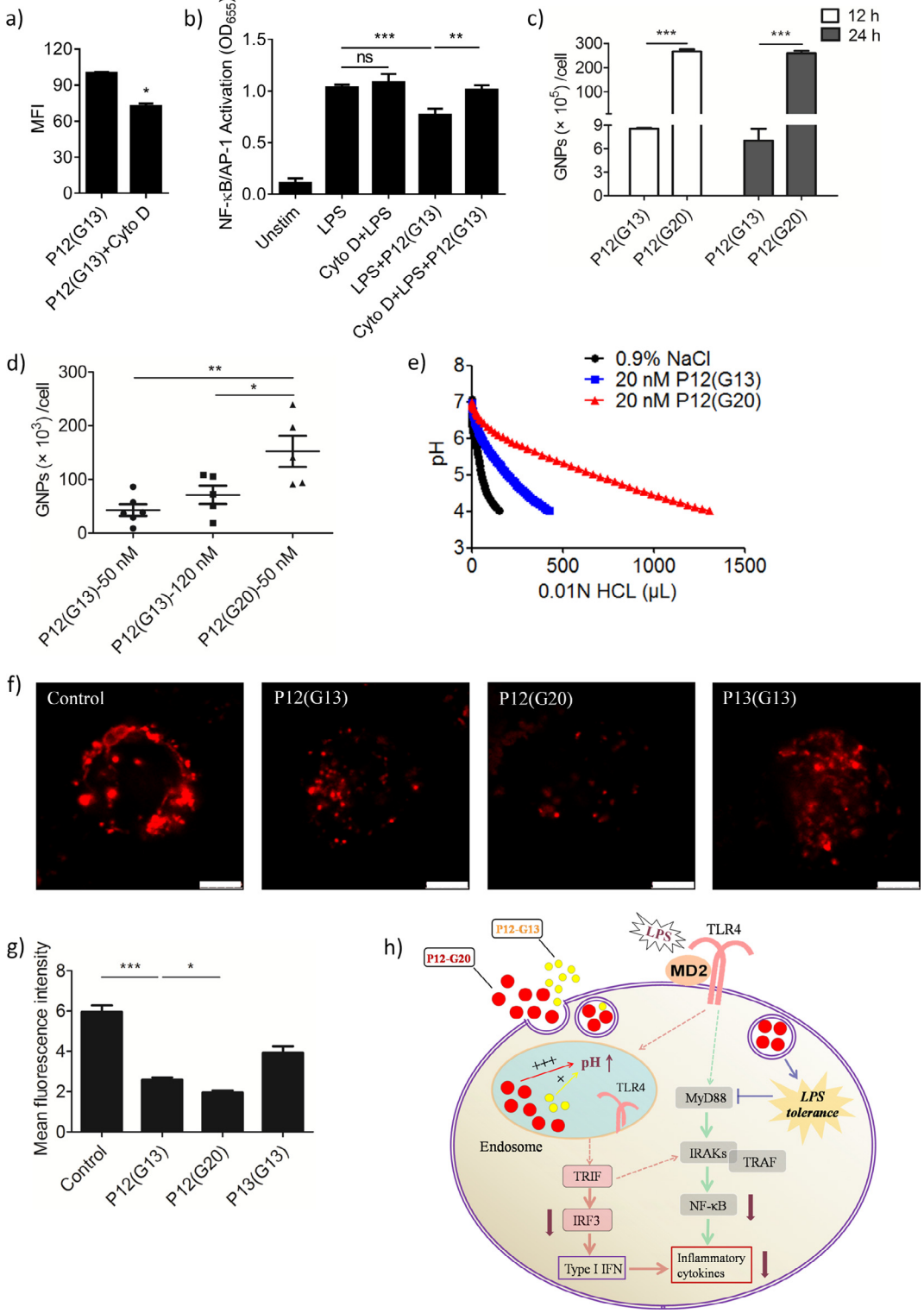

Fig. 8. Investigation of the mechanisms of action of the stronger anti-inflammatory effects by the larger hybrid P12(G20). (a) The reduction of cellular uptake of P12(G13) by the endocytosis inhibitor Cyto D (300 nM). (b) Inhibition of P12(G13) cellular uptake by Cyto D diminishing the anti-inflammatory activity of P12(G13) (25 nM). The quantification of the cellular uptake of various hybrids in THP-1 cell derived macrophages (c) and BAL macrophages (d) analyzed by ICP-MS. (e) pH titration curve of P12(G20) and P12(G13) in 0.9% NaCl solution. (f) Representative confocal images showing the nanoparticle size effect on blocking of the endosomal acidification by the hybrids in THP-1 derived macrophages. Endosomal pH was probed with the dye pHrodo red-dextran (red color). Scale bar represents 5 μm. P13(G13) as the inactive nanoparticle control. (g) Quantitative analysis of the red fluorescence intensity in the cells showing the changes in the endosomal pH upon the hybrid treatments. The mean fluorescence intensity was calculated from 30 to 50 cells per condition. (h) Illustration of the proposed mechanisms of stronger inhibitory activity of the hybrid P12(G20) on TLR4 activation. $N \geq 3$, $^{*}p < 0.05$, $^{**}p < 0.01$, $^{***}p < 0.001$. (For interpretation of the references to color in this figure legend, the reader is referred to the web version of this article.)

decreases (within a range of pH 4–8). As shown in Fig. 8f and g, both P12(G20) and P12(G13) treatments had dimmer red fluorescence comparing to the control; the red fluorescence of the P12 (G20) treated group was significantly lower than that of the P12 (G13) group. These results confirmed that P12(G20) was more effective in blocking the endosomal acidification process in the cells, and thereby exhibited more potent TLR4 inhibition comparing to P12(G13).

Based on the above findings, we proposed a hypothetical working model for the size enhanced anti-inflammatory activity of P12 (Fig. 8h). The larger hybrid P12(G20) had enhanced cellular uptake and more effective modulation of endosomal pH, resulting in more potent TLR4 inhibition; together with the ability to reinforce the LPS tolerance, P12(G20) exhibited the enhanced anti-inflammatory activity *in vitro* and better protective effects in a LPS-induced ALI model.

3. Discussion

3.1. Peptide-GNP hybrids as novel, potent TLR nano-inhibitors for treating ALI/ARDS

Mounting evidence has shown that resident alveolar macrophages play a central role in the initiation and progression of inflammation in ALI/ARDS [39–44]. In the early phase of the disease, macrophages are quickly activated by recognizing the microbial products and/or danger signals liberated from tissue injuries. These activated macrophages further drive the acute inflammatory responses *via* releasing inflammatory cytokines, recruiting circulating neutrophils and monocytes to the lungs, and interacting with other cells (lymphocytes, epithelial and endothelial cells) to boost the inflammatory responses. These inflammatory processes are critical for fighting the invading pathogens; however, uncontrolled overwhelming inflammation eventually leads to lung damage and pulmonary edema. Therefore, regulating TLR signaling pathways of the alveolar macrophages in the early phase of lung injury to shut down the detrimental inflammatory reactions represents a promising therapeutic strategy to treat ALI/ARDS.

Our developed peptide-GNP hybrid, P12 (P12(G13) or P12 (G20)), holds an immense potential as a novel promising treatment for inflammatory diseases with complex pathophysiology, such as ALI/ARDS for the following reasons. First, P12 can effectively inhibit TLR4 signaling in macrophages (Fig. 2). It also has a broad inhibitory activity on multiple TLR pathways (e.g., TLR2, TLR3 and TLR5) [31,33], making it a potent nano-inhibitor to intervene inflammatory diseases involving the over-activation of multiple TLRs. Second, P12 treatment *via* intratracheal instillation can alleviate LPS-induced lung inflammation and injury *in vivo*. In particular, P12 strongly inhibited neutrophil recruitment and chemokines production (KC and CCL2) in the lung (Fig. 4b–e), which are key inflammatory mediators during the initiation and progression of ALI. Moreover, P12 could reduce the alveolocapillary membrane permeability caused by inflammatory mediators (Fig. 4f-g and Fig. 5). Third, by increasing the GNP core size to 20 nm, P12(G20) significantly improved both short-term and long-term survival rate of mice exposed to lethal doses of LPS (Fig. 6). P12(G20) could also induce endotoxin tolerance (Fig. 7), which may contribute to the improved long-term survival. Fourth, the fabrication of peptide-GNP hybrids is simple and easy to scale up, and their size and surface properties can be finely controlled. These features and therapeutic activities make peptide-GNP hybrids promising candidates as novel "nanodrugs" for the treatments of many inflammatory conditions including ALI/ARDS.

Another attractive advantage of developing nanoparticle (NP)-based anti-inflammatory therapeutics to treat inflammatory diseases is the newly discovered "NanoEL" effect [45–50]. NanoEL effect states that nanomaterials can induce endothelial cell barrier leakiness by binding to the adherens junction protein VE–cadherin and disrupting the cell–cell interactions. Such an effect is expected to help intravenously administered nanodrugs cross the vascular barrier to the target sites, and assist the clearance of locally delivered nanodevices from the body through the blood circulation system. To date, a variety of nanomaterials has been found to exert NanoEL effect, including TiO_2 NPs, nanodiamonds, silica NPs and GNPs. For GNPs, interestingly it has been found that NPs with the size between 10 and 30 nm are good NanoEL inducing particles for air-blood barrier translocation [50]. In this study, we also found the leakage of our peptide-GNP hybrids from lungs to blood circulation and other organs (Fig. S7). Conceptually, it is very possible that the 'NanoEL' effect is involved in the clearance and translocation of the hybrids out of the lung, which would be advantageous for long-term safety.

3.2. Nanoparticle size-dependent modulation of TLR signaling in vitro and in vivo

It is well-known that the size of nanoparticles can significantly influence their bio-activities and interactions with biological systems [18,51]. This is mainly because the nanoparticle size has direct impacts on the surface area and interfacial properties, which in turn determines the capacity of carrying bio-active molecules, the strength of molecular binding to surroundings, and the fate after being internalized into a cell. A good example is that the binding affinity of Herceptin to its receptor becomes ~20 times higher when loaded onto a 10-nm nanoparticle; it is further enhanced over 30 times when the nanoparticle size increases from 10 nm to 70 nm [52]. Furthermore, numerous evidences have also shown that nanoparticles with a size around 30–50 nm appear to have an optimal cellular uptake in a variety of mammalian cells [53]; one possible reason for this phenomenon is that at these optimal sizes, the nanoparticles can be effectively wrapped around by the cell membranes to form vesicles for internalization. Equally important, the nanoparticle size significantly contributes to the *in vivo* biodistribution and pharmacokinetics as well [54]. It has been found that nanoparticles with a size of 10–100 nm display a longer circulation half-life and higher accumulation in the tumor, whereas larger nanoparticles (>100 nm) tend to accumulate in the liver and spleen, and smaller nanoparticles (<10 nm) can be easily excreted in urine. Therefore, it is crucial to investigate the effects of the nanoparticle size on the bio-activity for a given nano-system to improve the therapeutic outcomes and biosafety profiles for clinical translation.

In this work, we found that indeed the larger hybrid P12(G20) (vs. P12(G13) and P12(G5)) was more potent in inhibiting the LPS-induced NF-κB and IRF activation and the secretion of proinflammatory cytokines (CCL2, CCL4) in THP-1 derived macrophages (Fig. 2 and Fig. S4). This higher therapeutic efficacy was also found in a LPS-induced ALI mouse model (Figs. 4–6). Strikingly, P12(G20) could extend the survival of mice challenged with two lethal doses of LPS (Fig. 6). Such an effect could be attributed to the induction of a stronger LPS tolerance by P12(G20) (Fig. 7) (see below discussion).

The possible mechanism(s) of action behind the size-dependent enhancement of inhibiting TLR signaling and lung inflammation was likely due to a higher cellular uptake and stronger endosomal pH modulation at a larger size of the peptide-GNP hybrids (Fig. 8). The bigger GNPs (20 nm) supply a larger surface area for more peptides coating on the surface, contributing to more negative charges to neutralize the protons, thereby a higher capacity of endosomal pH modulation. In combination with its higher uptake into macrophages, P12(G20) exerted more efficient blockade of endosomal

acidification, and thus demonstrated more potent inhibition on NF-κB and IRF3 activation. It is worth noting that even at the same nanoparticle surface area (120-nM P12(G13) vs. 50-nM P12 (G20)), the larger hybrid P12(G20) still had a higher ability to prolong ALI mouse survival and induce LPS tolerance (Figs. 6 and 7). Altogether, these *in vitro* and *in vivo* experimental evidences suggested the importance of the nanoparticle size in modulating the anti-inflammatory activity of the peptide-GNP hybrids. Although the observed enhanced anti-inflammatory activity was found to be highly nanoparticle size-dependent, it should be clarified that nanoparticle size was not the "only" contributing factor. In fact, the nanoparticle size serves as an important fundamental factor that can influence other properties of the hybrids. For example, different nanoparticle sizes can affect the surface curvature and surface area as well as the capacity of the peptide loading; they all could ultimately contribute to the enhanced bio-activity of the hybrids. In addition to the nanoparticle size, we cannot exclude other possible mechanisms for the stronger anti-inflammatory effect of P12(G20) such as interacting with plasma membrane proteins or acting on autophagosome-mediated signaling [55,56].

It is worth noting that our hybrids may interact with plasma proteins to form a protein layer surrounding the hybrids, known as "protein corona". Protein corona has become an important factor affecting the therapeutic effects of nanoparticles administered intravenously. The formation of protein corona on a nanodevice will not only alter its original physicochemical properties, but also impart additional bio-activities linking to its (patho)biological implications and sometimes unexpected outcomes [46,57]. Interestingly, we did observe possible interaction of our hybrids with serum proteins for the reduced surface charge and increased hydrodynamic diameter of the hybrids in simulated physiological fluids (containing 5% FBS) (Table S1). Thus, there exists possibility that our hybrids may interact with some proteins in the surfactant layer in the alveoli after instilled into the lung. Accordingly, we could not exclude the possibility that protein corona might be another mechanism (in addition to high cellular uptake and endosomal pH modulation) contributing to the difference in anti-inflammatory activity of the hybrids with different GNP core sizes. We will employ proteomic technology to study this in the future.

3.3. Nano-enhanced LPS tolerance

LPS tolerance or ET is a transient state of irresponsiveness of innate immune cells (e.g., macrophages) that are pre-exposed to LPS under the second hit of LPS. Such phenomenon can be observed in the experimental settings of cultured cells and animal models as well as in clinical conditions of sepsis and trauma, indicating its pathophysiological significance and clinical relevance [58,59]. ET is an important protective mechanism adapted by the host to regulate the overwhelming inflammation from the endotoxin shock during infections [58]. Interestingly, ET can also fortify the host defense against infection, as the LPS tolerant mice had prolonged survival and reduced bacterial load [60]. However, exuberant ET is suggested to cause immune dysregulation and increase disease mortality often seen in sepsis patients [61]. Therefore, it is necessary to develop strategies to tightly regulate this process.

A number of strategies have been developed to manipulate ET *in vitro* and *in vivo*. For example, specific cytokines such as granulocyte macrophage-colony stimulating factor (GM-CSF) or interferon gamma (INF-γ) were found to be able to reverse the ET effect [62]; ET can also be diminished by the analgesic morphine through modulating the miR-146a [63]. On the other hand, tools have also been developed to enhance the ET effect for protection against excessive inflammation. Alpha-ketoglutarate (αKG) generated from glutamine metabolism was found to promote ET effect *via* Jmjd3-dependent metabolic and epigenetic reprogramming [64]. Herein, we reported a novel nano-based strategy to promote the ET effect, where the bigger hybrid P12(G20), but not P12(G13) could significantly enhance the LPS tolerance and provide both short-term and long-term protection for ALI mice challenged with lethal doses of LPS (Fig. 6). We suspected that such an ET effect by P12(G20) may be associated with its high cellular uptake, and perhaps interacting with certain proteins participating in the ET signaling. More studies are underway to disclose the possible mechanism(s) of action of LPS tolerance by P12(G20).

4. Conclusions

Building on our previous discovery of the anti-inflammatory peptide-GNP hybrid P12, we made a significant progress in enhancing its anti-inflammatory activities *in vitro* and *in vivo* by altering the size of the GNP core. Specifically, the 20-nm hybrid P12(G20) exhibited stronger inhibition on TLR4 activation and its downstream cytokines production (CCL2, CCL4) in THP-1 cell-derived macrophages than the 13-nm hybrid P12(G13) and 5-nm hybrid P12(G5). The enhanced inhibitory effects could be due to the higher cellular uptake and stronger endosomal pH buffering capacity of P12(G20). In a LPS-induced ALI mouse model, P12(G20) was able to better control the acute inflammation and reduce the injuries in the lungs. With large excitement, P12(G20) but not P12(G13), was found to significantly increase both short-term and long-term survival rates of mice under lethal LPS challenges, likely due to the enhanced LPS tolerance effect by P12(G20). Note that such an enhancement was not simply due to the increased surface area of the bigger 20-nm GNP core comparing to 13-nm GNP core. These findings demonstrated the importance of controlling the size of a nanodevice in amplifying its therapeutic activities and provided a size-dependent control of endotoxin tolerance to strategically treat ALI/ARDS or other TLR-associated inflammatory diseases.

5. Methods

5.1. Synthesis and characterization of the peptide-GNP hybrids

Gold nanoparticles (GNPs) (13 and 20 nm) were synthesized according to an improved method from the literature and our earlier work [31,65] while 5-nm, 30-nm, 40-nm and 50-nm GNPs were purchased from TedPella, Inc. (Redding, CA, USA). The preparation of peptide-GNP hybrids was conducted according to our earlier work [30,31]. Briefly, peptides (CanPeptide Inc., Montreal, Canada) were dissolved in ultrapure water as a stock solution of 1 mM. One volume of peptide solutions was mixed with ten volumes of the GNP solution under overnight incubation to allow peptide conjugation to the GNPs. To fabricate peptide-GNP hybrids with a higher peptide density, sodium chloride solution (NaCl, 3 M) was slowly added into the mixtures during peptide conjugation till a final NaCl concentration of 500 mM was reached. All peptide-GNP hybrid solutions were sterilized by filtration through a syringe filter (0.22 μm, Milipore, Billerica, MA, USA), and were handled in a biosafety cabinet to keep the solutions free from contamination. For free peptide ligands removal, the hybrid solutions were centrifuged (15,000 rpm at 4 °C for 30 min) and washed three times with sterile phosphate buffered saline (PBS). All hybrids were stable in PBS without aggregation except those with the GNP core size bigger than 20 nm.

The average diameter of bare GNPs and the peptide-GNP hybrids were measured by JEOL JEM-2100 electron microscope (Tokyo, Japan) at an accelerating voltage of 220 kV. The average hydrodynamic diameter of the bare GNPs and hybrids were determined by dynamic light scattering (DLS) on a Zetasizer (Malvern Instruments, Worcestershire, UK).

The stability of peptide-GNP hybrids at the physiological conditions was characterized following previously developed method [30]. Briefly, the hybrid solution was mixed with various concentrations of sodium chloride solution at 1:1 volume ratio in a 96-well plate and incubated for 2 h at room temperature. The optical density (OD) at 524 nm was measured with a plate reader (Varioskan Flash, Thermo Scientific, Waltham, USA). The data were normalized with the OD value in the absence of NaCl.

5.2. Cell culture and cytokine analysis

THP-1 cells were cultured in the complete RPMI-1640 medium containing 10% fetal bovine serum (FBS), 1 mM sodium pyruvate and 2 mM L-glutamine (Gibco, USA). Cells were treated with 50 ng/ml phorbol-12-myristate-13-acetate (PMA, Sigma Aldrich) for 24 h to differentiate into macrophage-like cells and then washed with PBS three times followed by 48-h rest. THP-1 derived macrophages were exposed to LPS (10 ng/mL) with or without various hybrids (50 nM or 100 nM). After 24 h incubation, culture medium was collected and centrifuged at 15,000 rpm, 4 °C for 30 min and the supernatants were stored at −80 °C prior to the cytokine analysis. The levels of macrophage chemotactic protein-1 (MCP-1/CCL2) and macrophage inflammatory protein 1-beta (MIP-1β/CCL4) in the supernatants were quantified by ELISA (eBioscience, San Diego, CA) following the manufacturer's instructions.

5.3. Reporter cell assay for the analysis of NF-κB/AP-1 and IRF activation

The reporter cells, THP1-XBlue and THP1-Blue ISG cells were purchased from InvivoGen (San Diedo, CA, USA). They were cultured using standard protocols described in our previous work [31]. Cells (10^5 cells/well) were seeded into a 96-well plate and differentiated into macrophages following the same procedure described above prior to the experiments. These macrophages were treated with LPS (10 ng/mL) in the presence or absence of different hybrids (P12(G13), P12(G20), P13(G13) or P13(G20)) with various concentrations (50, 100 or 120 nM) for 24 h. Culture media from each well were collected and centrifuged at 15000 rpm for 30 min and the supernatants were stored for further analysis.

For NF-κB/AP-1 activation, 20 μL supernatants from THP1-XBlue cells were incubated with 180 μL QUANTI-Blue solution at 37 °C for 1–2 h in a 96-well flat-bottom plate. For IRF activation, 20 μL supernatants from THP1-Blue ISG cells (IRF) were analyzed in the same way described above. The color change of the solution was quantified by analyzing the absorption at 655 nm on a microplate reader (SpectraMax iD3, Molecular Devices, Sunnyvale, CA, USA).

5.4. Immunoblotting

THP-1 cells (2×10^6 cells/well) were seeded in a 12-well plate and differentiated into macrophages. They were then treated with LPS (10 ng/mL) with or without various hybrids for different time periods up to 3 h. Whole cell lysates were prepared following the procedure reported in our earlier publication [32]. The protein concentrations were measured and adjusted using Bradford assay (Thermo Fisher Scientific, USA). Proteins were separated on 10% sodium dodecyl sulfate (SDS)-polyacrylamide gels and transferred to PVDF membranes (Immobilon-FL, EMD Millipore, Germany) after electrophoresis. The membranes were blocked with tris-buffered saline (G Biosciences) containing 5% bovine serum albumin (BSA, Sigma-Aldrich, USA) and 0.1% Tween 20 (Sigma-Aldrich) for 1 h at room temperature followed by staining with the primary antibodies, anti-phospho-p65, anti-IκBα, anti-β-actin, anti-GAPDH, anti-phospho-IRF3 and anti-IRF3 (all from Cell Signaling Technology USA), at 4 °C overnight. The blots were washed and incubated with fluorescently-labeled secondary antibodies, IRDye anti-rabbit 800CW and anti-mouse 680RD (LI-COR Biosciences, USA) for 1 h at room temperature. Blots were imaged on a LI-COR Odyssey infrared imaging system (LI-COR Biosciences).

5.5. Intracellular pH assay and confocal imaging

THP-1 cells (2×10^5 cells/well) were seeded and differentiated into macrophages in 8-well chamber slides. They were incubated with pHrodo red-labeled 10,000 MW dextrans (10 μg/ml) (Life Technologies), together with P12(G13) (50 nM), P12(G20) (50 nM) or P13(G13) (50 nM) for 6 h. Cells were then washed with PBS three times and imaged on a Leica SP5 confocal microscope (Leica Microsystems Inc., Wetzlar, Germany). The fluorescence of pHrodo red (excitation 565/emission 585) within the cells was quantified by Image J software. For each condition, a minimum of 30 cells from 3 independent experiments were quantified.

5.6. Acid-base titration of the peptide-GNP hybrids

The buffering effect of the hybrids P12(G13) and P12(G20) was examined by a standard acid-base titration method [66]. P12(G13) and P12(G20) at concentration of 20 nM were re-suspended in a 0.9% NaCl solution. The 0.9% NaCl solution was also used as a control. All solutions were first adjusted to pH 7, and then titrated by stepwise addition of 0.01 N HCl solution until pH reached 4. The titration profile was made by plotting the solution pH against the accumulated volume of the added HCl solution.

5.7. Nanoparticle cellular uptake assay

THP-1 cells (5×10^5 cells/well) were seeded in a 24-well plate and differentiated into macrophages. They were treated with various hybrids (50 nM) for 12 and 24 h. Cells were first rinsed with ice-cold PBS 3 times to remove extracellular nanoparticles, and then detached through vigorously pipetting with 1 mL ice-cold PBS containing 2 mM EDTA. The cell suspensions were centrifuged at 300 × g for 5 min and washed with PBS twice again. The cell pellets were dissolved in a mixture of 8 mL nitric (GR, Sinopharm Chemical Reagent Co, Ltd) and 2 mL perchloric acid (GR, Sinopharm Chemical Reagent Co, Ltd). The above solution was sat for 15 min at room temperature and then heated at 70 °C for 1 h until the cell pellets were totally dissolved to form a clear solution (final volume of 1 mL). All samples were further diluted using 2% Aqua Regia (nitric acid: hydrochloric acid of 1:3), and the amount of Au were analyzed using an ICP-MS instrument (iCAP Q, Thermo Fisher Scientific, Bremen, Germany). The data were shown as number of GNPs per 100,000 cells.

For evaluating the effect of the endocytosis inhibitor cytochalasin D (Sigma) on the uptake of P12(G13), THP-1 cell derived macrophages were pretreated with PBS control or cytochalasin D (300 nM) for 0.5 h, and then treated with the Cy5-PEG5000-SH (0.5%, Nanocs Inc.) labeled P12(G13) for 3 h in the absence or presence of cytochalasin D (300 nM). The cells were then washed three times with cold PBS and collected for flow cytometry analysis (BD Accuri C6, BD Biosciences). The mean fluorescence intensity (MFI) of Cy5 was calculated, representing the cellular uptake of P12 (G13).

5.8. LPS-induced acute lung injury (ALI) murine model

The experimental protocol of ALI mouse model was performed according to protocols approved by the Shanghai Jiaotong University Affiliated First People's Hospital Institutional Animal Care and Use Committee guidelines for the care and use of laboratory animals (Approval number # 2018KY201).

The 7–8-week-old male C57BL/6 mice were purchased from Shanghai Laboratory Animal Co. Ltd. (Shanghai, China). All the procedure was conducted under sodium pentobarbital anesthesia, and all efforts were made to minimize mouse suffering. Hybrid treatments (500 nM, 50 μL) or PBS negative control were intratracheally instilled using a laryngoscope and a bent gavage needle at 1 h prior to intranasal LPS challenge (10 mg/kg body weight, 50 μL) or PBS as a control [67]. Mice were sacrificed 24 h after LPS challenge for the analysis of lung inflammation and injury.

5.9. Bronchoalveolar lavage fluid (BALF) analysis

Bronchoalveolar lavage (BAL) was performed by tracheotomy and injecting 0.8 mL cold PBS through the trachea, followed by carefully withdrawing. The volume of retrieved fluid was >60% of the injected one. BAL cells were collected by centrifuging the BALF at 1200 rpm for 10 min at 4 °C and then resuspended in PBS solution. Total number of cells were counted on a hemocytometer with trypan blue exclusion. Aliquots of the BALF were cytocentrifuged onto a glass slide and stained with Wright-Giemsa (Baso Diagnostics, Inc. Zhuhai, China). The differential cell counts were determined by counting 200 cells under 400× magnification. Meanwhile, the BALF supernatants were stored in −80 °C freezer until further cytokine analysis. The release of keratinocyte chemoattractant (KC) and CCL2 in BALF were analyzed by ELISA kits (eBioscience) according to the manufacturer's instructions. The BAL total protein was measured by BCA-protein quantification assay kit (Beyotime, Shanghai, China). BAL cells were fluorescently labelled with CD11b (clone M1/70, Biolegend) and F4-80 (clone BM8, Biolegend) antibodies, and $CD11b^{+}F4\text{-}80^{+}$cells (macrophages) were sorted out by Flow for the uptake analysis in BAL macrophages by ICP-MS.

5.10. Histological analysis and lung W/D ratio

In a separate set of mice, the left lung lobe of mice was dissected and fixed in 10% buffered formalin and embedded into paraffin. The samples were processed to obtain 4 μm paraffin sections on glass slides, which were stained with hematoxylin and eosin (H&E), followed by dehydrating and mounting. The sample sections were imaged and subjected to lung injury assessment by two independent investigators who were blinded to the sample groups using a scoring system described previously [68]. To assess lung injury, six randomly chosen fields of each section were evaluated based on five independent variables: neutrophils in the alveolar space, neutrophils in the interstitial space, hyaline membranes, proteinaceous debris filling the airspaces and alveolar septal thickening. For a given field, each variable is scored with 0, 1 or 2 according to the injury severity. The variables were then weighted differently based on their relevance to the lung injury. The sum of the weighted variables was averaged by the number of determined fields, resulting in the final score with a value between 0 and 1 [68].

Right lungs of mice from each group were collected and weighed. They were then placed in an oven at 60 °C for approximately 48 h to dry the tissues prior to the second weighing. The weight ratio of wet and dry (W/D) lung was then calculated.

5.11. Survival curve

In a different experimental set-up, mice (at least 8 mice per each group) were under a lethal dose (20 mg/kg) of LPS challenge intranasally to induce severe ALI. The survival and weight loss of mice in each group were recorded every day for 7 days. Mice that survived from the first LPS shock were re-challenged with an even higher dose (25 mg/kg) of LPS on Day 11 from the first challenge. Mice were continuously monitored for survival every day for another week, and the experiment was ended on Day 17.

5.12. Statistical analysis

Statistical analysis was performed using GraphPad Prism 7. Results were compared by one-way or two-way ANOVA with a Bonferroni post-test whenever applicable. P value <0.05 was considered statistically significant. Data were expressed as means ± SEM with $N \geq 3$.

Acknowledgements

This work was financially supported by the National Natural Science Foundation of China (No. 81770070 for HY and 81870064 for QL). HY also would like to acknowledge the support from the Program for Professor of Special Appointment (Eastern Scholar) at Shanghai Institutions of Higher Learning (TP2016014), Shanghai Municipal Education Commission – Gaofeng Clinical Medicine Grant Support (20171923) and the starting fund from Shanghai General Hospital.

Disclosures

The authors declare that there is no conflict of interest in relation to this submission.

Appendix A. Supplementary data

Supplementary data to this article can be found online at https://doi.org/10.1016/j.actbio.2018.12.046.

References

[1] M.A. Matthay, R.L. Zemans, The acute respiratory distress syndrome: pathogenesis and treatment, Ann. Rev. Pathol-Mech. 6 (2011) 147–163.
[2] G.D. Rubenfeld, E. Caldwell, E. Peabody, J. Weaver, D.P. Martin, M. Neff, E.J. Stern, L.D. Hudson, Incidence and outcomes of acute lung injury, New Engl. J. Med. 353 (16) (2005) 1685–1693.
[3] J.F. Tomashefski, Pulmonary pathology of acute respiratory distress syndrome, Clin. Chest Med. 21 (3) (2000) 435–466.
[4] M.A. Matthay, L.B. Ware, G.A. Zimmerman, The acute respiratory distress syndrome, J. Clin. Invest. 122 (8) (2012) 2731–2740.
[5] L.B. Tolle, T.J. Standiford, Danger-associated molecular patterns (DAMPs) in acute lung injury, J. Pathol. 229 (2) (2013) 145–156.
[6] B. Beutler, A. Poltorak, Sepsis and evolution of the innate immune response, Crit. Care Med. 29 (7) (2001) S2–S6.
[7] D. Jiang, J. Liang, Y. Li, P.W. Noble, The role of Toll-like receptors in non-infectious lung injury, Cell Res. 16 (8) (2006) 693–701.
[8] W. Gao, Y. Xiong, Q. Li, H. Yang, Inhibition of Toll-like receptor signaling as a promising therapy for inflammatory diseases: a journey from molecular to nano therapeutics, Front. Physiol. 8 (2017) 508.
[9] N. Matsunaga, N. Tsuchimori, T. Matsumoto, M. Ii, TAK-242 (resatorvid), a small-molecule inhibitor of toll-like receptor (TLR) 4 signaling, binds selectively to TLR4 and interferes with interactions between TLR4 and its adaptor molecules, Mol. Pharmacol. 79 (1) (2011) 34–41.
[10] A. Barochia, S. Solomon, X.Z. Cui, C. Natanson, P.Q. Eichacker, Eritoran tetrasodium (e5564) treatment for sepsis: review of preclinical and clinical studies, Expert Opin. Drug Metab. Toxicol. 7 (4) (2011) 479–494.
[11] E. Monnet, G. Lapeyre, E.V. Poelgeest, P. Jacqmin, K. Graaf, J. Reijers, M. Moerland, J. Burggraaf, C. Min, Evidence of NI-0101 pharmacological activity, an anti-TLR4 antibody, in a randomized phase I dose escalation study in healthy volunteers receiving LPS, Clin. Pharmacol. Ther. 101 (2) (2017) 200–208.
[12] K.D. Taganov, M.P. Boldin, K.J. Chang, D. Baltimore, NF-κB-dependent induction of microRNA miR-146, an inhibitor targeted to signaling proteins of innate immune responses, Proc. Natl. Acad. Sci. USA 103 (33) (2006) 12481–12486.
[13] S.Y. Fung, T. Oyaizu, H. Yang, Y.F. Yuan, B. Han, S. Keshavjee, M.Y. Liu, The potential of nanoscale combinations of self-assembling peptides and amino acids of the src tyrosine kinase inhibitor in acute lung injury therapy, Biomaterials 32 (16) (2011) 4000–4008.
[14] D.P. Patterson, A. Rynda-Apple, A.L. Harmsen, A.G. Harmsen, T. Douglas, Biomimetic antigenic nanoparticles elicit controlled protective immune response to influenza, ACS Nano 7 (4) (2013) 3036–3044.

[15] Z. Hunter, D.P. McCarthy, W.T. Yap, C.T. Harp, D.R. Getts, L.D. Shea, S.D. Miller, A biodegradable nanoparticle platform for the induction of antigen-specific immune tolerance for treatment of autoimmune disease, ACS Nano 8 (3) (2014) 2148–2160.
[16] K. Ariga, T. Mori, J. Li, Langmuir nanoarchitectonics from basic to frontier, Langmuir (2018) (online).
[17] K. Ariga, Y. Yamauchi, K.C. Wu, A special section on nanoarchitectonics, J. Nanosci. Nanotechnol. 18 (1) (2018) 1–2.
[18] N. Hoshyar, S. Gray, H.B. Han, G. Bao, The effect of nanoparticle size on in vivo pharmacokinetics and cellular interaction, Nanomedicine 11 (6) (2016) 673–692.
[19] E.C. Dreaden, L.A. Austin, M.A. Mackey, M.A. El-Sayed, Size matters: gold nanoparticles in targeted cancer drug delivery, Ther. Deliv. 3 (4) (2012) 457–478.
[20] L. Tang, J. Azzi, M. Kwon, M. Mounayar, R. Tong, Q. Yin, R. Moore, N. Skartsis, T. M. Fan, R. Abdi, J. Cheng, Immunosuppressive activity of size-controlled PEG-PLGA nanoparticles containing encapsulated cyclosporine A, J. Transplant. 2012 (2012) 896141.
[21] P. Bannas, J. Hambach, F. Koch-Nolte, Nanobodies and nanobody-based human heavy chain antibodies as antitumor therapeutics, Front. Immunol. 8 (2017) 1603.
[22] Z. Zhou, A. Chan, Z. Wang, X. Huang, G. Yu, O. Jacobson, S. Wang, Y. Liu, L. Shan, Y. Dai, Z. Shen, L. Lin, W. Chen, X. Chen, Synchronous chemoradiation nanovesicles by x-ray triggered cascade of drug release, Angew. Chem. Int. Ed. Engl. 57 (28) (2018) 8463–8467.
[23] J. Dernedde, A. Rausch, M. Weinhart, S. Enders, R. Tauber, K. Licha, M. Schirner, U. Zugel, A. von Bonin, R. Haag, Dendritic polyglycerol sulfates as multivalent inhibitors of inflammation, Proc. Natl. Acad. Sci. USA 107 (46) (2010) 19679–19684.
[24] F. Aline, D. Brand, J. Pierre, P. Roingeard, M. Severine, B. Verrier, I. Dimier-Poisson, Dendritic cells loaded with HIV-1 p24 proteins adsorbed on surfactant-free anionic PLA nanoparticles induce enhanced cellular immune responses against HIV-1 after vaccination, Vaccine 27 (38) (2009) 5284–5291.
[25] D.R. Getts, L.D. Shea, S.D. Miller, N.J. King, Harnessing nanoparticles for immune modulation, Trends Immunol. 36 (7) (2015) 419–427.
[26] R.M. Pearson, L.M. Casey, K.R. Hughes, S.D. Miller, L.D. Shea, In vivo reprogramming of immune cells: technologies for induction of antigen-specific tolerance, Adv. Drug. Deliv. Rev. 114 (2017) 240–255.
[27] H. Babazada, F. Yamashita, M. Hashida, Suppression of experimental arthritis with self-assembling glycol-split heparin nanoparticles via inhibition of TLR4-NF-κB signaling, J. Control. Release 194 (2014) 295–300.
[28] H. Babazada, F. Yamashita, S. Yanamoto, M. Hashida, Self-assembling lipid modified glycol-split heparin nanoparticles suppress lipopolysaccharide-induced inflammation through TLR4-NF-κB signaling, J. Control. Release 194 (2014) 332–340.
[29] L. Foit, C.S. Thaxton, Synthetic high-density lipoprotein-like nanoparticles potently inhibit cell signaling and production of inflammatory mediators induced by lipopolysaccharide binding Toll-like receptor 4, Biomaterials 100 (2016) 67–75.
[30] H. Yang, S.Y. Fung, M. Liu, Programming the cellular uptake of physiologically stable peptide-gold nanoparticle hybrids with single amino acids, Angew. Chem. Int. Ed. Engl. 50 (41) (2011) 9643–9646.
[31] H. Yang, S.Y. Fung, S. Xu, D.P. Sutherland, T.R. Kollmann, M. Liu, S.E. Turvey, Amino acid-dependent attenuation of Toll-like receptor signaling by peptide-gold nanoparticle hybrids, ACS Nano 9 (7) (2015) 6774–6784.
[32] H. Yang, L. Kozicky, A. Saferali, S.Y. Fung, N. Afacan, B. Cai, R. Falsafi, E. Gill, M. Liu, T.R. Kollmann, R.E. Hancock, L.M. Sly, S.E. Turvey, Endosomal pH modulation by peptide-gold nanoparticle hybrids enables potent anti-inflammatory activity in phagocytic immune cells, Biomaterials 111 (2016) 90–102.
[33] H. Yang, S.Y. Fung, A. Bao, Q. Li, S.E. Turvey, Screening bioactive nanoparticles in phagocytic immune cells for inhibitors of toll-like receptor signaling, J. Vis. Exp. 125 (2017).
[34] H. Yang, Y. Zhou, S.Y. Fung, W. Licun, K. Tsai, R. Tan, S.E. Turvey, T. Machuca, M. de Perrot, T.K. Waddell, M. Liu, Amino acid structure determines the immune responses generated by peptide-gold nanoparticle hybrids, Part. Part. Syst. Charact. 30 (12) (2013) 1039–1043.
[35] J.C. Kagan, T. Su, T. Horng, A. Chow, S. Akira, R. Medzhitov, TRAM couples endocytosis of Toll-like receptor 4 to the induction of interferon-β, Nat. Immunol. 9 (4) (2008) 361–368.
[36] O. de Bouteiller, E. Merck, U.A. Hasan, S. Hubac, B. Benguigui, G. Trinchieri, E.E. Bates, C. Caux, Recognition of double-stranded RNA by human Toll-like receptor 3 and downstream receptor signaling requires multimerization and an acidic pH, J. Biol. Chem. 280 (46) (2005) 38133–38145.
[37] M. Rutz, J. Metzger, T. Gellert, P. Luppa, G.B. Lipford, H. Wagner, S. Bauer, Toll-like receptor 9 binds single-stranded CpG-DNA in a sequence- and pH-dependent manner, Eur. J. Immunol. 34 (9) (2004) 2541–2550.
[38] G. Las, S.B. Serada, J.D. Wikstrom, G. Twig, O.S. Shirihai, Fatty acids suppress autophagic turnover in beta-cells, J. Biol. Chem. 286 (49) (2011) 42534–42544.
[39] N.R. Aggarwal, L.S. King, F.R. D'Alessio, Diverse macrophage populations mediate acute lung inflammation and resolution, Am. J. Physiol. Lung. Cell Mol. Physiol. 306 (8) (2014) L709–L725.
[40] B.T. Thompson, R.C. Chambers, K.D. Liu, Acute respiratory distress syndrome, N Engl. J. Med. 377 (6) (2017) 562–572.
[41] J. Villar, A.S. Slutsky, Golden anniversary of the acute respiratory distress syndrome: still much work to do! Curr. Opin. Crit Care 23 (1) (2017) 4–9.
[42] E. Festic, D.J. Kor, O. Gajic, Prevention of acute respiratory distress syndrome, Curr. Opin. Crit Care 21 (1) (2015) 82–90.
[43] R.G. Spragg, G.R. Bernard, W. Checkley, J.R. Curtis, O. Gajic, G. Guyatt, J. Hall, E. Israel, M. Jain, D.M. Needham, A.G. Randolph, G.D. Rubenfeld, D. Schoenfeld, B. T. Thompson, L.B. Ware, D. Young, A.L. Harabin, Beyond mortality: future clinical research in acute lung injury, Am. J. Respir. Crit. Care Med. 181 (10) (2010) 1121–1127.
[44] D.J. Kor, R.E. Carter, P.K. Park, E. Festic, V.M. Banner-Goodspeed, R. Hinds, D. Talmor, O. Gajic, L.B. Ware, M.N. Gong, U.S.C. Illness, G., Injury Trials Group: Lung Injury Prevention with Aspirin Study, Effect of aspirin on development of ards in at-risk patients presenting to the emergency department: the LIPS-A randomized clinical trial, JAMA 315 (22) (2016) 2406–2414.
[45] M.I. Setyawati, C.Y. Tay, S.L. Chia, S.L. Goh, W. Fang, M.J. Neo, H.C. Chong, S.M. Tan, S.C.J. Loo, K.W. Ng, J.P. Xie, C.N. Ong, N.S. Tan, D.T. Leong, Titanium dioxide nanomaterials cause endothelial cell leakiness by disrupting the homophilic interaction of VE-cadherin, Nat. Commun. 4 (10) (2013) 1673–1684.
[46] C.Y. Tay, M.I. Setyawati, J.P. Xie, W.J. Parak, D.T. Leong, Back to basics: exploiting the innate physico-chemical characteristics of nanomaterials for biomedical applications, Adv. Funct. Mater. 24 (38) (2014) 5936–5955.
[47] M.I. Setyawati, C.Y. Tay, D. Docter, R.H. Stauber, D.T. Leong, Understanding and exploiting nanoparticles' intimacy with the blood vessel and blood, Chem. Soc. Rev. 44 (22) (2015) 8174–8199.
[48] M.I. Setyawati, V.N. Mochalin, D.T. Leong, Tuning endothelial permeability with functionalized nanodiamonds, ACS nano 10 (1) (2016) 1170–1181.
[49] C.Y. Tay, M.I. Setyawati, D.T. Leong, Nanoparticle density: a critical biophysical regulator of endothelial permeability, ACS nano 11 (3) (2017) 2764–2772.
[50] M.I. Setyawati, C.Y. Tay, B.H. Bay, D.T. Leong, Gold nanoparticles induced endothelial leakiness depends on particle size and endothelial cell origin, ACS nano 11 (5) (2017) 5020–5030.
[51] A. Albanese, P.S. Tang, W.C.W. Chan, The effect of nanoparticle size, shape, and surface chemistry on biological systems, Annu. Rev. Biomed. Eng. 14 (14) (2012) 1–16.
[52] W. Jiang, B.Y.S. Kim, J.T. Rutka, W.C.W. Chan, Nanoparticle-mediated cellular response is size-dependent, Nat. Nanotechnol. 3 (3) (2008) 145–150.
[53] A. Malugin, H. Ghandehari, Cellular uptake and toxicity of gold nanoparticles in prostate cancer cells: a comparative study of rods and spheres, J. Appl. Toxicol. 30 (3) (2010) 212–217.
[54] S.D. Li, L. Huang, Pharmacokinetics and biodistribution of nanoparticles, Mol. Pharmaceut. 5 (4) (2008) 496–504.
[55] C.Y. Tsai, S.L. Lu, C.W. Hu, C.S. Yeh, G.B. Lee, H.Y. Lei, Size-dependent attenuation of TLR9 signaling by gold nanoparticles in macrophages, J. Immunol. 188 (1) (2012) 68–76.
[56] V. Deretic, T. Saitoh, S. Akira, Autophagy in infection, inflammation and immunity, Nat. Rev. Immunol. 13 (10) (2013) 722–737.
[57] M.I. Setyawati, C.Y. Tay, D. Docter, R.H. Stauber, D.T. Leong, Understanding and exploiting nanoparticles' intimacy with the blood vessel and blood, Chem. Soc. Rev. 44 (22) (2015) 8174–8199.
[58] S.K. Biswas, E. Lopez-Collazo, Endotoxin tolerance: new mechanisms, molecules and clinical significance, Trends Immunol. 30 (10) (2009) 475–487.
[59] C.S. Deutschman, K.J. Tracey, Sepsis: current dogma and new perspectives, Immunity 40 (4) (2014) 463–475.
[60] M.D. Lehner, J. Ittner, D.S. Bundschuh, N. van Rooijen, A. Wendel, T. Hartung, Improved innate immunity of endotoxin-tolerant mice increases resistance to salmonella enterica serovar typhimurium infection despite attenuated cytokine response, Infect. Immun. 69 (1) (2001) 463–471.
[61] J.M. Cavaillon, C. Adrie, C. Fitting, M. Adib-Conquy, Endotoxin tolerance: is there a clinical relevance? J. Endotoxin. Res. 9 (2) (2003) 101–107.
[62] M. Adib-Conquy, J.M. Cavaillon, Gamma interferon and granulocyte/monocyte colony-stimulating factor prevent endotoxin tolerance in human monocytes by promoting interleukin-1 receptor-associated kinase expression and its association to MyD88 and not by modulating TLR4 expression, J. Biol. Chem. 277 (31) (2002) 27927–27934.
[63] S. Banerjee, J.J. Meng, S. Das, A. Krishnan, J. Haworth, R. Charboneau, Y. Zeng, S. Ramakrishnan, S. Roy, Morphine induced exacerbation of sepsis is mediated by tempering endotoxin tolerance through modulation of miR-146a, Sci. Rep. 3 (2013) 1977.
[64] P.S. Liu, H. Wang, X. Li, T. Chao, T. Teav, S. Christen, G. Di Conza, W.C. Cheng, C. H. Chou, M. Vavakova, C. Muret, K. Debackere, M. Mazzone, H.D. Huang, S.M. Fendt, J. Ivanisevic, P.C. Ho, Alpha-ketoglutarate orchestrates macrophage activation through metabolic and epigenetic reprogramming, Nat. Immunol. 18 (9) (2017) 985–994.
[65] R.E.J.J. Storhoff, R.C. Mucic, C.A. Mirkin, R.L. Letsinger, One-pot colorimetric differentiation of polynucleotides with single base imperfections using gold nanoparticle probes, J. Am. Chem. Soc. 120 (1998) 1959–1964.
[66] Y. Dong, J. Yang, H. Liu, T. Wang, S. Tang, J. Zhang, X. Zhang, Site-specific drug-releasing polypeptide nanocarriers based on dual-pH response for enhanced therapeutic efficacy against drug-resistant tumors, Theranostics 5 (8) (2015) 890–904.
[67] M. Rayamajhi, E.F. Redente, T.V. Condon, M. Gonzalez-Juarrero, D.W. Riches, L. L. Lenz, Non-surgical intratracheal instillation of mice with analysis of lungs and lung draining lymph nodes by flow cytometry, J. Vis. Exp. (2011) 51.
[68] G. Matute-Bello, G. Downey, B.B. Moore, S.D. Groshong, M.A. Matthay, A.S. Slutsky, W.M. Kuebler, An official american thoracic society workshop report: features and measurements of experimental acute lung injury in animals, Am. J. Respir. Cell Mol. Biol. 44 (5) (2011) 725–738.